




Nociceptor sensory neurons suppress neutrophil and $\gamma\delta$ T cell responses in bacterial lung infections and lethal pneumonia

Pankaj Baral¹, Benjamin D Umans² , Lu Li³, Antonia Wallrapp⁴, Meghna Bist¹, Talia Kirschbaum¹, Yibing Wei¹, Yan Zhou¹, Vijay K Kuchroo⁴, Patrick R Burkett^{4,5}, Bryan G Yipp³ , Stephen D Liberles² & Isaac M Chiu¹ 

Lung-innervating nociceptor sensory neurons detect noxious or harmful stimuli and consequently protect organisms by mediating coughing, pain, and bronchoconstriction. However, the role of sensory neurons in pulmonary host defense is unclear. Here, we found that TRPV1⁺ nociceptors suppressed protective immunity against lethal *Staphylococcus aureus* pneumonia. Targeted TRPV1⁺-neuron ablation increased survival, cytokine induction, and lung bacterial clearance. Nociceptors suppressed the recruitment and surveillance of neutrophils, and altered lung $\gamma\delta$ T cell numbers, which are necessary for immunity. Vagal ganglia TRPV1⁺ afferents mediated immunosuppression through release of the neuropeptide calcitonin gene-related peptide (CGRP). Targeting neuroimmunological signaling may be an effective approach to treat lung infections and bacterial pneumonia.

The lung is a major barrier surface that interfaces with the environment and is often prone to infection. A highly coordinated immune response protects the respiratory tract from pathogens and other external insults. The role of the nervous system in regulating pulmonary host defense is not well defined. Pulmonary infections and lethal pneumonia are major public-health problems frequently causing death in children and immunocompromised and elderly people¹. *S. aureus* is a Gram-positive human bacterial pathogen that is the leading cause of hospital-acquired infections, particularly respiratory-tract infections and ventilator-associated pneumonia^{1–4}. The increased prevalence of multidrug-resistant bacteria including methicillin-resistant *S. aureus* (MRSA) strains necessitates nonantibiotic approaches to treatment. Targeting neuroimmunological signaling may be a novel approach to boost host immunity against lung pathogens.

The trachea, bronchi, and airways are innervated by peripheral sensory afferents originating from vagal and spinal sensory neurons, whose cell bodies reside within the vagal ganglia (VG) and dorsal root ganglia (DRG), respectively^{5–7}. Nociceptor neurons are the subset of these neurons that respond to noxious stimuli including heat, protons, ATP, mechanical injury, inflammation, and chemical irritants⁸. Upon activation, nociceptors induce pain, coughing, and bronchoconstriction^{5,8–10}. Recent work has shown that nociceptors cross-talk with immune cells in the respiratory tract, thereby driving allergic responses and bronchoconstriction in mouse models of asthma^{5,11,12}. Here, we investigated a previously unexplored role of sensory neurons in pulmonary host defenses against bacterial invasion and lethal pneumonia.

RESULTS

TRPV1⁺ neurons mediate survival and bacterial clearance in pneumonia

We hypothesized that lung-innervating nociceptors are poised to detect bacterial invasion and to coordinate pulmonary immunity. The Transient receptor potential vanilloid 1 (TRPV1) ion channel responds to capsaicin, protons, and heat stimuli^{8,13}. TRPV1 is expressed by many C fibers, including nociceptors that mediate thermal nociception and inflammatory hyperalgesia^{14–16}. TRPV1⁺ neurons have been found to drive allergic airway hypersensitivity⁵.

We first used a genetic approach to determine the role of TRPV1⁺ neurons in host defense^{5,16}. *Trpv1-Dtr* mice express the human diphtheria-toxin receptor (DTR) under control of mouse TRPV1 regulatory sequences¹⁶. Mouse cells are normally resistant to diphtheria toxin (DT)-induced apoptosis but are rendered susceptible by expression of DTR. We performed daily injections of DT into 5- to 7-week old *Trpv1-Dtr* mice to selectively ablate TRPV1⁺ neurons^{5,16}. DT treatment, compared with PBS treatment, significantly ablated TRPV1⁺ neurons in both the DRG and VG in *Trpv1-Dtr* mice (**Supplementary Fig. 1**). CGRP is expressed by many peptidergic C-fiber nociceptors^{16,17}. There were significantly fewer CGRP⁺ neurons in DT-treated *Trpv1-Dtr* mice than in PBS-treated controls (**Supplementary Fig. 1**). In contrast, the proportion of NF-200⁺ neurons, which include A fibers, was higher in the DT-treated *Trpv1-Dtr* mice. In DT-treated compared with PBS-treated *Trpv1-Dtr* mice, we also observed a loss of CGRP⁺ nerves around the airways (**Supplementary Fig. 2**) and

¹Department of Microbiology and Immunobiology, Division of Immunology, Harvard Medical School, Boston, Massachusetts, USA. ²Department of Cell Biology, Harvard Medical School, Boston, Massachusetts, USA. ³Department of Critical Care, Cumming School of Medicine, University of Calgary, Calgary, Alberta, Canada. ⁴Evergrande Center for Immunologic Diseases, Harvard Medical School and Brigham and Women's Hospital, Boston, Massachusetts, USA. ⁵Division of Pulmonary and Critical Care Medicine, Department of Medicine, Brigham and Women's Hospital, Boston, Massachusetts, USA. Correspondence should be addressed to I.M.C. (isaac_chiu@hms.harvard.edu).

Received 14 August 2017; accepted 16 January 2018; published online 5 March 2018; corrected online 16 July 2018; doi:10.1038/nm.4501

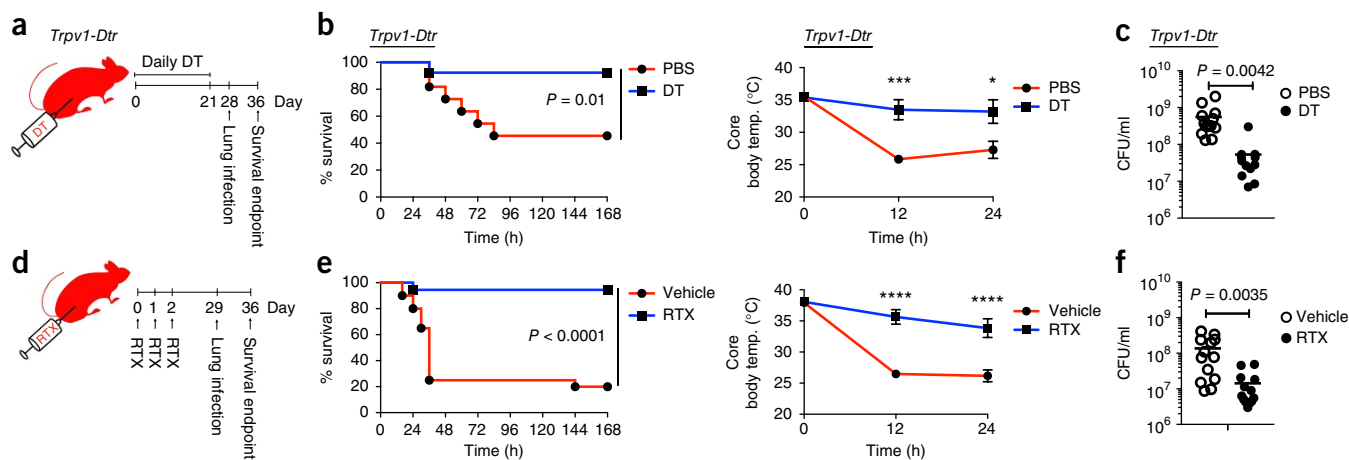


Figure 1 TRPV1 neurons regulate survival and the outcome of lethal *S. aureus* pneumonia. **(a)** For genetic ablation of TRPV1⁺ neurons, *Trpv1-Dtr* mice 5 to 7 weeks of age were treated with DT (200 ng/mouse intraperitoneally (i.p.)) daily for 21 d. Mice were rested 7 d before intratracheal inoculation with *S. aureus* USA300 (1.3×10^8 to 1.4×10^8 CFU/mouse). **(b)** Left, survival curves of PBS-treated *Trpv1-Dtr* mice ($n = 11$) and DT-treated *Trpv1-Dtr* mice ($n = 13$). Log-rank (Mantel-Cox) test ($P = 0.01$). Right, measurements of core body temperature (temp.) over time in PBS-treated ($n = 7$) and DT-treated *Trpv1-Dtr* mice ($n = 8$). Two-way repeated (RM) analysis of variance (ANOVA) with Bonferroni post tests (** $P = 0.001$; * $P = 0.014$). **(c)** Lung bacterial burdens 12 h after infection in PBS-treated ($n = 13$) and DT-treated *Trpv1-Dtr* mice ($n = 12$). Two-tailed unpaired t test ($P = 0.0042$). **(d)** Resiniferatoxin (RTX)-mediated chemical ablation of TRPV1⁺ neurons. WT mice 4 weeks of age were injected subcutaneously daily with three escalating doses of RTX or vehicle. Mice were rested for 4 weeks before intratracheal inoculation with *S. aureus* USA300 (0.8×10^8 to 1×10^8 CFU/mouse). **(e)** Left, survival curves of vehicle-treated ($n = 20$) and RTX-treated mice ($n = 18$). Log-rank test ($P < 0.0001$). Right, core-body-temperature measurements in vehicle-treated ($n = 5$) and RTX-treated mice ($n = 5$). Two-way RM ANOVA with Bonferroni post tests (**** $P < 0.001$). **(f)** Lung bacterial-load recovery 12 h after *S. aureus* infection in vehicle-treated ($n = 13$) and RTX-treated mice ($n = 13$). Two-tailed unpaired t tests ($P = 0.0035$). Data were pooled from two **(b)** or three **(c, e, f)** independent experiments. Data are shown as mean \pm s.e.m. **(b, e, f)** core body temperature and mean **(c, f)**.

decreased noxious-heat responses in hot-plate and tail-flick assays (Supplementary Fig. 3).

Next, we asked whether TRPV1⁺ neurons might affect pulmonary host defenses. *Trpv1-Dtr* mice recovered 7 d after DT or PBS treatment and were subsequently intratracheally inoculated with a lethal dose of the MRSA strain USA300 (1.3×10^8 to 1.4×10^8 colony-forming units (CFU); Fig. 1a). *Trpv1-Dtr* mice treated with DT, compared with those treated with PBS, showed significantly longer survival and better maintenance of core body temperature after MRSA pneumonia (Fig. 1b). DT-treated *Trpv1-Dtr* mice, compared with PBS-treated controls, also exhibited tenfold-lower bacterial burdens recovered from lungs at 12 h postinfection (Fig. 1c).

We used Resiniferatoxin (RTX) as a second strategy to target TRPV1⁺ neurons. RTX is a high-affinity TRPV1 ligand that can be used to chemically denervate and ablate nociceptors^{15,18}. Mice were subcutaneously treated with RTX at 4 weeks of age for consecutive days with escalating doses (30, 70, and 100 μ g/kg) according to established protocols^{19,20}. RTX-treated mice, compared with vehicle-treated mice, showed increased latency to noxious heat in hot-plate and tail-flick assays, and loss of TRPV1⁺ and CGRP⁺ neurons in the DRG and VG (Supplementary Figs. 3 and 4). At 4 weeks after RTX injection, mice were intratracheally inoculated with MRSA (0.8×10^8 to 1×10^8 CFU; Fig. 1d). Whereas most vehicle-treated mice succumbed to pneumonia (80% mortality), most RTX-treated mice survived (Fig. 1e). RTX-treated mice, compared with vehicle-treated mice, showed improved maintenance of core body temperature (Fig. 1e) and less lung bacterial burden (Fig. 1f). *Trpv1-Dtr*-mediated ablation and RTX treatment enhanced protection in mice infected with a sublethal dose of *S. aureus* (2×10^7 to 4×10^7 CFU), as measured by bacterial-load recovery (Supplementary Fig. 5). Because nociceptors may regulate the peripheral resistance of the cardiovascular and pulmonary systems

to infection, we measured vital signs. However, the oxygen saturation, heart rate, perfusion, and respiratory rates did not differ between RTX-treated and vehicle-treated mice at steady state; the respiratory rates also did not differ postinfection (Supplementary Fig. 6).

Next, we asked whether nociceptors might modulate host defense against bacterial pathogens other than *S. aureus*. RTX-treated and vehicle-treated mice were infected with lethal doses of *Streptococcus pneumoniae*, *Klebsiella pneumoniae*, or *Pseudomonas aeruginosa*. The RTX-treated mice and vehicle-treated mice showed similar decreases in core body temperature after infection with the three pathogens (Supplementary Fig. 7). Nociceptor deficiency showed a modest but nonsignificant protective effect ($P = 0.13$) in survival during *S. pneumoniae* infection (Supplementary Fig. 7). Nociceptor deficiency did not affect death caused by *K. pneumoniae* or *P. aeruginosa* pneumonia (Supplementary Fig. 7).

Nav1.8 is a voltage-gated sodium channel expressed by a large subset of nociceptors that overlap with but are distinct from TRPV1⁺ neurons^{16,21}. *Nav1.8-cre^{+/-}* mice were bred with diphtheria toxin A (DTA) reporter mice to generate animals deficient in Nav1.8-lineage neurons (*Nav1.8-Cre^{+/-}; Dta*)²¹. After MRSA infection, we observed a trend toward higher survival ($P = 0.09$) and lower bacterial burden ($P = 0.07$) in *Nav1.8-Cre^{+/-}; Dta* mice than in control littermates (Supplementary Fig. 8). However, the beneficial effects of Nav1.8-lineage neuron ablation (Supplementary Fig. 8) were considerably smaller than those observed for TRPV1 neuron ablation (Fig. 1).

TRPV1 ion channel does not mediate pulmonary host defense

We next determined whether the TRPV1 ion channel itself was involved in host defense. *Trpv1^{-/-}* mice have previously been found to have exaggerated physiologic responses in a model of polymicrobial sepsis²². After *S. aureus* lung infection, we did not observe

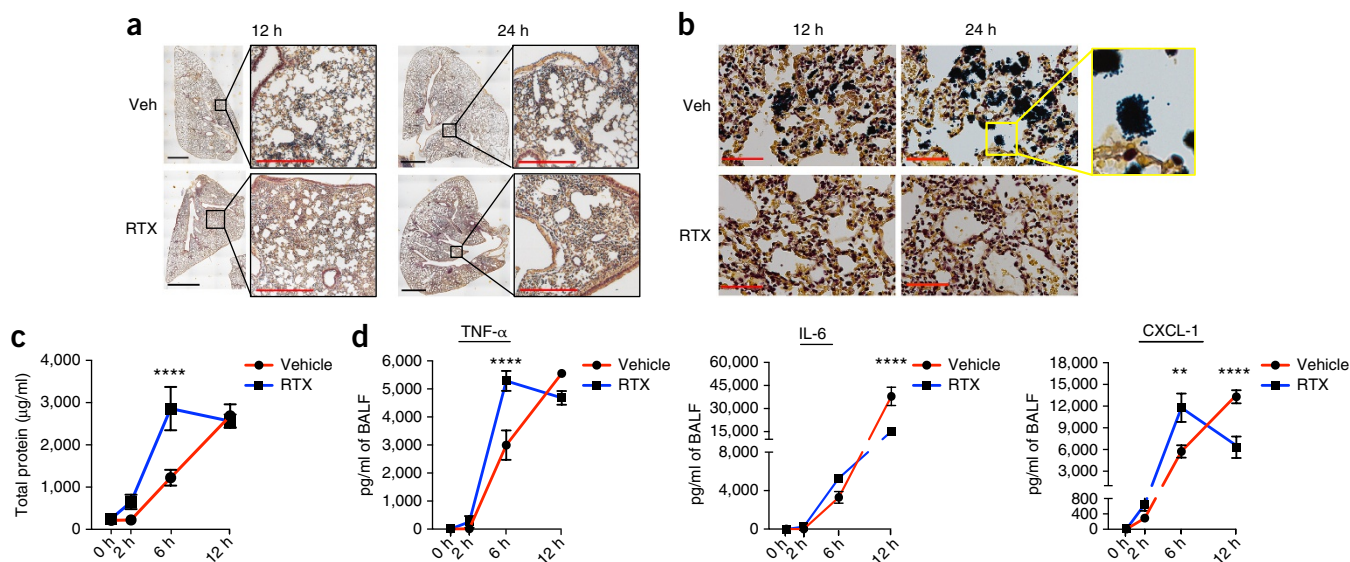


Figure 2 TRPV1 neurons suppress lung inflammation and cytokine induction during *S. aureus* infection. (a) H&E-stained lung sections from vehicle-treated and RTX-treated mice at 12 h or 24 h after *S. aureus* infection. Representative images were chosen from 15 lung lobes imaged from 3 mice in each group (vehicle (veh) and RTX). Scale bars: black, 500 µm; red, 100 µm. (b) Brown and Brenn Gram-stained images of bacterial colonies in lung sections from vehicle-treated and RTX-treated mice, 12 h and 24 h after infection. Representative images were chosen from 15 lung lobes imaged from 3 mice in each group (vehicle and RTX). Inset, purple bacterial cocci are *S. aureus* colonies. Red scale bars, 50 µm. (c) Quantification of total protein levels in BALF at different time points after *S. aureus* infection (1×10^8 CFU/mouse). Vehicle-treated group, 0 h ($n = 6$), 2 h ($n = 8$), 6 h ($n = 8$), 12 h ($n = 9$); RTX-treated group, 0 h ($n = 6$), 2 h ($n = 7$), 6 h ($n = 6$), 12 h ($n = 10$). Two-way RM ANOVA with Bonferroni post tests (**** $P < 0.001$). (d) Levels of IL-6, TNF- α , and CXCL-1 in BALF from mice at different time points after *S. aureus* infection (1×10^8 CFU/mouse). TNF- α : vehicle-treated group, 0 h ($n = 6$), 2 h ($n = 10$), 6 h ($n = 10$), 12 h ($n = 10$); RTX-treated group, 0 h ($n = 6$), 2 h ($n = 7$), 6 h ($n = 6$), 12 h ($n = 10$). IL-6: vehicle-treated group, 0 h ($n = 6$), 2 h ($n = 10$), 6 h ($n = 10$), 12 h ($n = 10$); RTX-treated group, 0 h ($n = 6$), 2 h ($n = 7$), 6 h ($n = 6$), 12 h ($n = 10$). CXCL-1: vehicle-treated group, 0 h ($n = 6$), 2 h ($n = 8$), 6 h ($n = 8$), 12 h ($n = 10$); RTX-treated group, 0 h ($n = 6$), 2 h ($n = 7$), 6 h ($n = 6$), 12 h ($n = 10$). Statistical analysis for all cytokines by two-way RM ANOVA with Bonferroni post tests (** $P = 0.0013$; **** $P < 0.0001$). Data from one experiment with multiple biological replicates are shown in a and b; data pooled from two independent experiments are shown in c and d. Data are shown as mean \pm s.e.m. in c and d.

significant differences in survival, core-body-temperature measurements, or lung bacterial burdens in *Trpv1*^{-/-} mice compared with *Trpv1*^{+/-} or *Trpv1*^{+/+} control littermates (Supplementary Fig. 9). The postinfection induction of cytokines (IL-17A, IL-6, and IL-23) in lung lysates of *Trpv1*^{-/-} mice was similar to that in control littermates (Supplementary Fig. 10). We also examined the role of TRPA1, which mediates airway inflammation in a mouse model of asthma¹¹. *Trpa1*^{-/-} mice, compared with *Trpa1*^{+/+} littermates, did not show differences in bacterial burdens after lethal or sublethal *S. aureus* infection (Supplementary Fig. 11).

TRPV1 and Nav1.8 neurons regulate bacterial dissemination

We next determined whether nociceptors mediated the spread of bacterial pathogens from the lung to extrapulmonary sites. DT-treated *Trpv1-Dtr* mice showed higher numbers of bacteria in the blood ($P = 0.01$) after lethal MRSA infection than did controls (Supplementary Fig. 12). RTX-treated mice also showed greater blood dissemination than did vehicle-treated controls (Supplementary Fig. 12). At a sublethal dose of infection, both *Trpv1-Dtr* ablation and RTX treatment increased MRSA dissemination to the blood and spleen (Supplementary Fig. 13). In *Nav1.8-Cre*^{+/-}; *Dta* mice, compared with control littermates, we also observed significantly greater bacterial dissemination to the blood, which was accompanied by greater spleen size (Supplementary Fig. 13). We investigated whether nociceptor ablation affected lung-barrier permeability. RTX-treated mice, compared with vehicle-treated mice, showed greater leakage of fluorescein

isothiocyanate (FITC)-dextran to the blood after intratracheal inoculation, thus suggesting a role of nociceptors in maintaining barrier integrity (Supplementary Fig. 14).

TRPV1 neurons regulate lung inflammation and cytokine induction

We performed histological analysis of lungs at different time points to analyze pulmonary inflammation after *S. aureus* infection. RTX-treated mice, compared with vehicle-treated mice, showed greater immune-cell influx in the lungs at 12 h and 24 h postinfection, as determined by H&E staining (Fig. 2a). We hypothesized that early increases in immune cells might correlate with improved bacterial clearance in RTX-treated mice. Brown and Brenn staining showed many Gram-positive bacterial colonies in vehicle-treated lungs at 12 h and 24 h postinfection (Fig. 2b). In contrast, RTX-treated mice showed few bacterial colonies (Fig. 2b). We next determined whether nociceptors regulated proinflammatory-cytokine production. At an early time point of infection (6 h), RTX-treated mice showed higher induction of total inflammatory-protein levels in the bronchoalveolar lavage fluid (BALF) (Fig. 2c), as well as levels of the cytokine TNF- α and the chemokine CXCL-1 (Fig. 2d). By 12 h postinfection, TNF- α , IL-6, and CXCL-1 levels were lower in RTX-treated mice (Fig. 2d), as were levels of the cytokines IL-1 β and MCP-1 (Supplementary Fig. 15). These data indicated that TRPV1⁺ neuron ablation leads to faster induction and resolution of cytokine levels during infection.

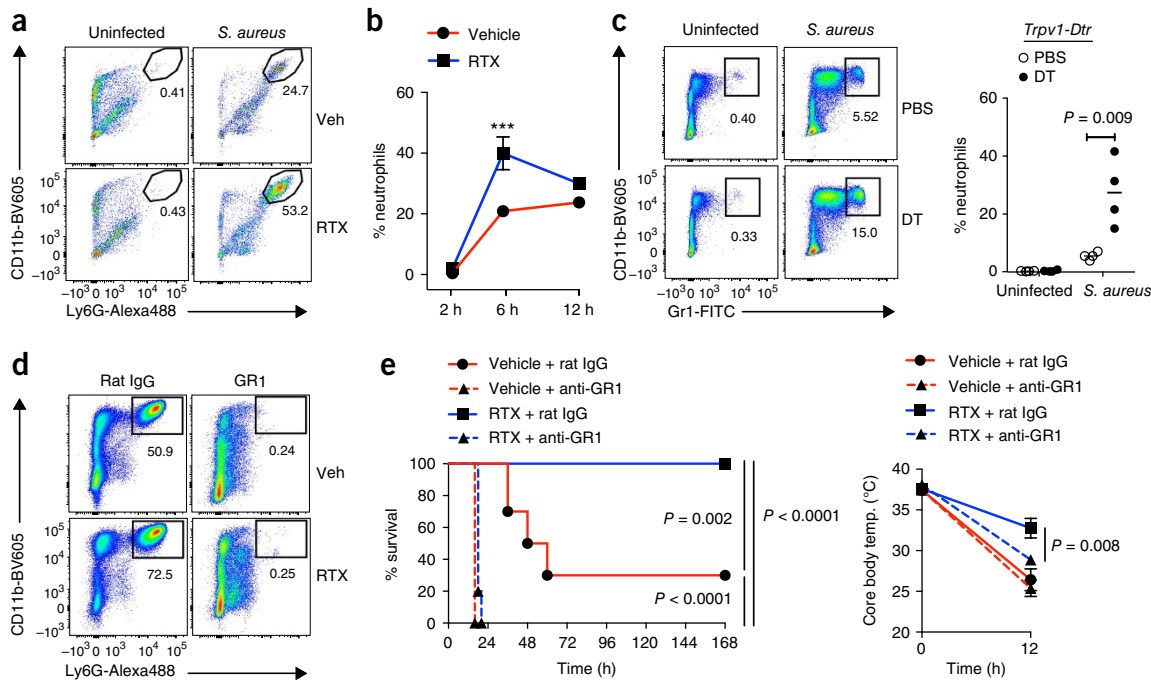


Figure 3 TRPV1 neurons suppress recruitment of Ly6G⁺ neutrophils essential for host defense against lethal pneumonia. **(a)** Representative FACS plots of neutrophils (CD11b⁺Ly6G⁺, out of CD45⁺ cells) in vehicle-treated and RTX-treated mice in BALF collected at 6 h postinfection with *S. aureus* (0.8×10^8 CFU/mouse). Representative FACS plots were chosen from 4 mice in each group (vehicle and RTX). **(b)** Time course of CD11b⁺Ly6G⁺ neutrophil recruitment in the BALF of RTX-treated mice compared with vehicle-treated mice after lethal *S. aureus* infection. $n = 4$ mice in each group (vehicle and RTX) for 2 h, 6 h, and 12 h data sets. Two-way ANOVA with Bonferroni post tests ($***P = 0.001$). **(c)** Representative FACS plots (left) and quantification data (right), showing neutrophils (Gr1^{hi}CD11b⁺ cells) in the lung homogenates of DT-treated ($n = 4$) and PBS-treated *Trpv1-Dtr* mice ($n = 4$) 12 h after *S. aureus* infection (1.3×10^8 CFU/mouse). Statistical analysis by two-tailed *t* test. **(d)** FACS plots showing anti-GR1 antibody-mediated ablation of lung neutrophils in vehicle ($n = 3$) and RTX-treated ($n = 3$) mice 12 h after *S. aureus* infection (0.8×10^8 CFU/mouse). **(e)** Left, Kaplan-Meier survival curves after *S. aureus* lung infection (1.2×10^8 to 1.35×10^8 CFU/mouse) of vehicle + rat IgG mice ($n = 10$), vehicle + anti-GR1 mice ($n = 10$), RTX + rat IgG mice ($n = 9$), and RTX + anti-GR1 mice ($n = 10$). Statistical analysis by log-rank test, $P < 0.0001$ (RTX + rat IgG versus RTX + anti-GR1), $P < 0.0001$ (vehicle + rat IgG versus vehicle + anti-GR1), and $P = 0.002$ (vehicle + rat IgG versus RTX + rat IgG). Right, core body temperature, measured after *S. aureus* infection with or without neutrophil depletion. Vehicle + rat IgG ($n = 5$); vehicle + anti-GR1 ($n = 5$); RTX + rat IgG ($n = 4$); RTX + anti-GR1 ($n = 5$). Statistical analysis by two-way RM ANOVA with Bonferroni post tests ($P = 0.008$, RTX + rat IgG versus RTX + anti-GR1). Data from two independent experiments (**b,e**) or one experiment with multiple biological replicates (**c**) are shown. Data are shown as mean \pm s.e.m. in **b, c** (neutrophil proportions), and **e** (core body temperature).

TRPV1 neurons suppress recruitment of neutrophils

We next used FACS analysis to analyze the kinetics of immune-cell influx into inflamed lungs during *S. aureus* infection. RTX-treated mice, compared with vehicle-treated mice, displayed greater CD11b⁺Ly6G⁺ lung neutrophil recruitment at 6 h and 12 h postinfection (Fig. 3a,b). *Trpv1-Dtr*-neuron-ablated mice showed greater neutrophil recruitment than did PBS-treated controls at 12 h postinfection (Fig. 3c). Because neutrophils are critical for bacterial clearance²³, we hypothesized that neuronal modulation of neutrophil recruitment might play a major role in MRSA pneumonia. We depleted neutrophils in RTX-treated mice by using low-dose anti-GR1 antibody treatment, which, compared with control IgG treatment, eliminated CD11b⁺Ly6G⁺ neutrophils in infected lungs (Fig. 3d). Anti-GR1 also decreased CD11b⁺Ly6C^{hi} monocytes but did not affect CD11b⁺Ly6C^{lo} monocytes (Supplementary Fig. 16). Neutrophil depletion in RTX-treated mice significantly increased their susceptibility to MRSA pneumonia: whereas 100% of anti-GR1-treated RTX mice succumbed to infection, 0% of the control IgG-treated RTX mice died from infection (Fig. 3e). These experimental results were confirmed in an independent cohort of mice (Supplementary Fig. 17). Neutrophils were also required for baseline protection

against MRSA pneumonia (Fig. 3e). These data suggested that RTX-mediated enhancement of lung immunity requires neutrophils.

TRPV1 neurons regulate pulmonary neutrophil surveillance

Within lungs, neutrophils perform endothelial and parenchymal surveillance for pathogens^{24,25}. Using intravital microscopy, we analyzed the subpleural vascular bed to assess whether neutrophil kinetics and patrolling of tissues were regulated by nociceptors. Compared with control mice, RTX-treated mice recruited significantly more neutrophils to pulmonary capillaries during early *S. aureus* pneumonia (Fig. 4a,b and Supplementary Video 1). We observed less GFP-*S. aureus* in the lungs of nociceptor-depleted animals, in agreement with previous CFU data. Dynamic neutrophil behavioral phenotypes were analyzed for tethering, crawling, and firm adhesion within the vasculature. Tethering is a rapid, transient neutrophil interaction with the vessel wall, which requires limited cellular activation. Adhesion indicates a more advanced state of activation mediated by integrins before tissue emigration. Crawling is a complex intravascular behavior that requires upregulation of $\beta 2$ -integrin, which occurs rapidly during lung host defense^{24,25}. Neutrophils behaved differently during host defense in control versus RTX-treated mice. In RTX-treated

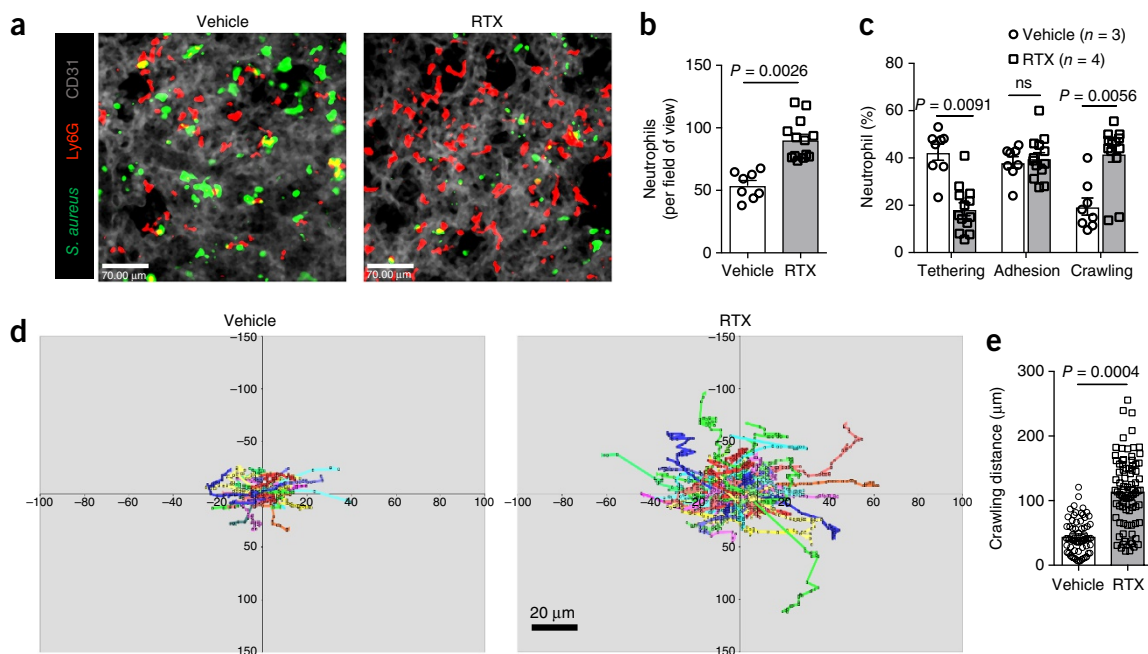


Figure 4 Neutrophil dynamics are altered in TRPV1-neuron-ablated mice. (a) *In vivo* imaging of neutrophils in the lungs after lethal GFP-*S. aureus* USA300 lung infection in live vehicle-treated and RTX-treated mice at 4 h postinfection. (b) Total neutrophils, determined per field of view. (c) Neutrophil behavior, phenotyped and quantified as tethering, adhesion, or crawling. NS, nonsignificant. (d) Crawling tracks, displayed for individual neutrophils. (e) Distances for individual neutrophils. *n* = 3 individual experiments performed for vehicle-treated mice and 4 individual experiments for RTX-treated mice. For statistical analyses, values for each parameter (b,c,e) were averaged for each animal, and two-tailed unpaired *t* tests were performed, comparing vehicle-treated and RTX-treated mouse groups. Data are shown as mean \pm s.e.m. in b, c, and e.

mice, a significant proportion of neutrophils demonstrated vascular crawling (Fig. 4c), and tracking individual pulmonary vascular neutrophils revealed significantly greater crawling distances (Fig. 4d,e), a phenotype consistent with cellular activation and host defense against bacterial pathogens. Therefore, live imaging supports the contention that enhanced neutrophil function in the absence of nociceptors aids in the eradication of bacterial pneumonia.

Nociceptor neurons regulate lung-resident $\gamma\delta$ T cells

We next asked whether TRPV1⁺ neurons might alter the lung-resident immune-cell populations in naive mice, thus setting the stage for subsequent inflammatory responses. We first examined immunological-transcriptome data sets at the Immunological Genome Project (<http://www.immgen.org/>) and found that *Trpv1* expression was absent across immune-cell types (Supplementary Fig. 18). Analysis of a second transcriptional data set²⁶ showed that *Trpv1* was absent in immune cells but was highly expressed in DRG (Supplementary Fig. 18). We next purified CD4⁺ T cells, B cells, neutrophils, and $\gamma\delta$ T cells from mouse lungs, and performed quantitative PCR analysis for *Trpv1* compared with that in sensory ganglia. Whereas *Trpv1* was highly expressed in the VG and DRG, it was undetectable in all lung immune cells analyzed (Supplementary Figs. 19 and 20). These data indicated that *Trpv1-Dtr* or RTX-mediated ablation should specifically target nociceptors but should not have direct effects on immune cells. We examined spleens of RTX-treated and vehicle-treated mice and did not observe differences in the populations of B220⁺ B cells, NK1.1⁺ cells, CD4⁺ T cells, CD8⁺ T cells, or $\gamma\delta$ T cells; moreover, *Trpv1-Dtr*-neuron-ablated mice showed similar results (Supplementary Fig. 21).

We next examined whether lung-resident immune-cell types differed in nociceptor-ablated mice at steady state. CD11b⁺ dendritic cells (CD11b⁺SiglecF⁻CD24⁻CD103⁻F4/80⁻MHCII⁺), CD103⁺

dendritic cells (CD11b⁻SiglecF⁻CD103⁺MHCII⁺), alveolar macrophages (SiglecF⁺CD11c⁺CD64⁺F4/80⁺), and interstitial macrophages (CD11b⁺CD24⁻CD64⁺F4/80⁺) did not differ between RTX-treated and vehicle-treated mice (Supplementary Fig. 22 and Fig. 5a). B cells, natural killer cells, and CD8⁺ T cells also did not differ; however, CD4⁺ T cells were slightly higher in RTX-treated mice than in controls (Supplementary Fig. 23 and Fig. 5b).

We observed higher absolute numbers of lung-resident $\gamma\delta$ T cells, in contrast to most other immune-cell types, in RTX-treated mice compared with vehicle-treated mice (Fig. 5c). Further subset analysis revealed that this increase was specific to V γ 1⁺ cells and V γ 1⁻V γ 2⁻ cells, but not V γ 2⁺ cells (Fig. 5c and Supplementary Figs. 24 and 25). We found a similar increase in $\gamma\delta$ T cells in *Nav1.8-Cre^{+/+}; Dta* mice compared with control littermates (Supplementary Fig. 24). $\gamma\delta$ T cells reside within epithelial layers of the lungs, skin, and gut, where they act as first responders to infection²⁷. We next used $\gamma\delta$ T cell-deficient *Tcrd^{-/-}* mice to investigate the role of these cells in neuroimmunological suppression. Wild-type (WT) or *Tcrd^{-/-}* mice were treated with RTX to ablate TRPV1⁺ neurons, and then *S. aureus* pneumonia was induced (Fig. 5d,e). The absence of $\gamma\delta$ T cells was confirmed in *Tcrd^{-/-}* mice through flow cytometry (Fig. 5d). *Tcrd* deficiency led to a loss of protection against MRSA infection and abrogated the survival enhancement due to RTX treatment (Fig. 5e). This reversal of protective immunity correlated with an imbalance in core body temperature (Fig. 5e) and greater bacterial burdens in BALF isolated from RTX-treated *Tcrd^{-/-}* mice compared with RTX-treated WT mice (Supplementary Fig. 26). *Tcrd^{-/-}* also showed defective baseline immunity against MRSA pneumonia (Fig. 5e). Whereas IL-6 levels were unaffected by *Tcrd* deficiency, levels of IL17A, a cytokine mediating protection against MRSA²⁸, were significantly lower in *Tcrd^{-/-}* mice (Supplementary Fig. 26). Neutrophil recruitment did

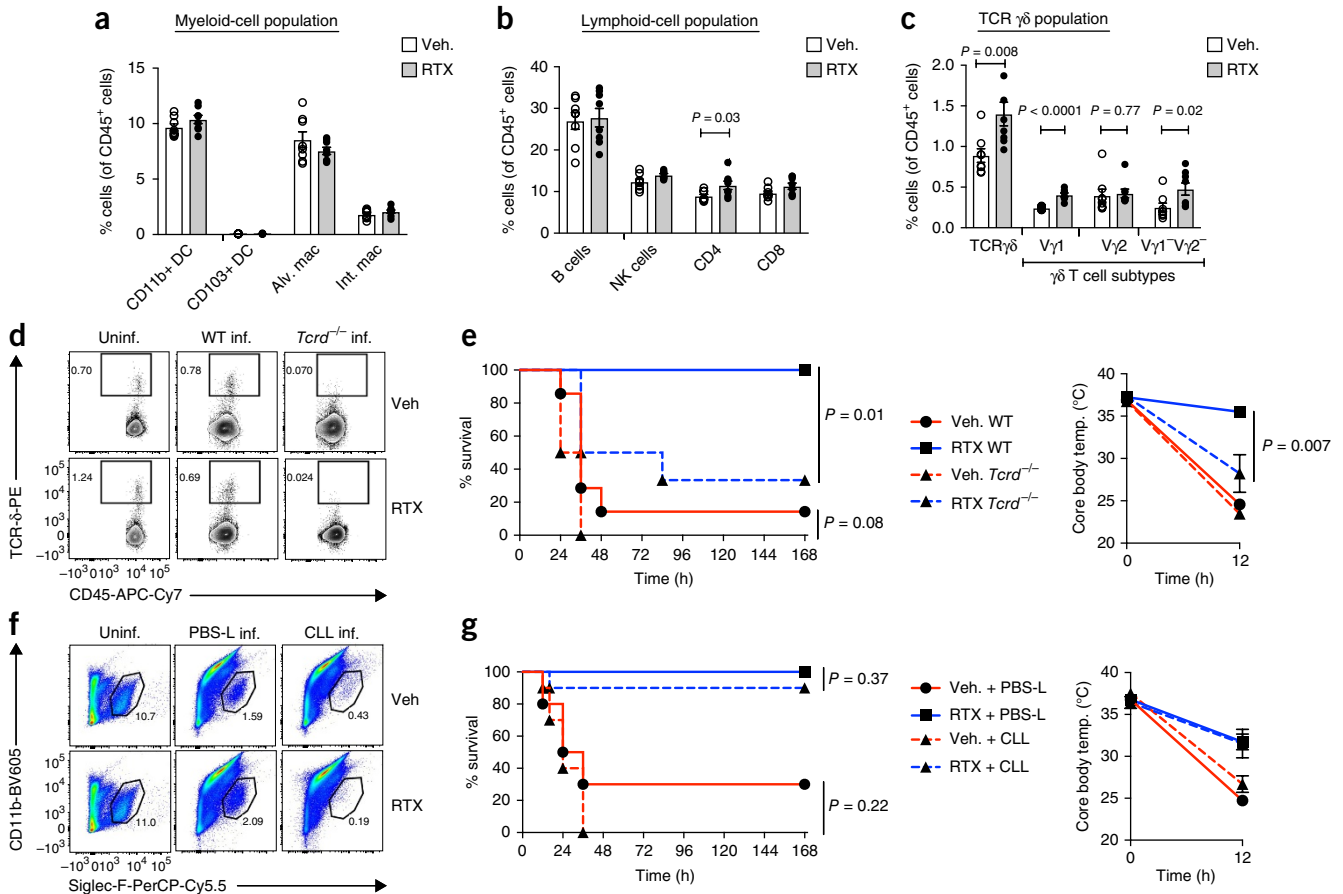


Figure 5 TRPV1 neurons regulate lung $\gamma\delta$ T cells, which mediate host protection against *S. aureus* pneumonia. (**a–c**) To detect differences at steady state, lung tissues from nociceptor-depleted (RTX treated, $n = 8$) and nondepleted mice (vehicle treated, $n = 8$) were analyzed by flow cytometry for myeloid immune cells (**a**), lymphoid immune cells (**b**), and $\gamma\delta$ T cell populations (**c**). Statistical analysis in **a–c** by two-tailed unpaired *t* tests. Alv. mac, alveolar macrophages; int. mac, interstitial macrophages; NK, natural killer. (**d**) Representative FACS plots showing $\gamma\delta$ T cells in WT or *Tcrd*^{-/-} mice (RTX or vehicle treated) either uninfected (uninf.) or 12 h postinfection (inf.) with *S. aureus* (1×10^8 CFU/mouse). Vehicle-treated groups: WT uninfected ($n = 8$), WT infected ($n = 4$), *Tcrd*^{-/-} infected ($n = 3$); RTX-treated groups: WT uninfected ($n = 8$), WT infected ($n = 4$), *Tcrd*^{-/-} infected ($n = 3$). (**e**) Left, survival curves for vehicle-treated WT mice ($n = 7$), vehicle-treated *Tcrd*^{-/-} mice ($n = 6$), RTX-treated WT mice ($n = 5$), and RTX-treated *Tcrd*^{-/-} mice ($n = 6$) after lethal *S. aureus* infection (1×10^8 CFU/mouse). Statistical analysis by log-rank test ($P = 0.01$, RTX-treated WT versus RTX-treated *Tcrd*^{-/-}; $P = 0.08$, vehicle-treated WT versus vehicle-treated *Tcrd*^{-/-}). Right, core-body-temperature measurements in vehicle-treated WT mice ($n = 5$), vehicle-treated *Tcrd*^{-/-} mice ($n = 5$), RTX-treated WT mice ($n = 5$), and RTX-treated *Tcrd*^{-/-} mice ($n = 4$). Two-way RM ANOVA with Bonferroni post tests ($P < 0.0001$, RTX-treated WT versus RTX-treated *Tcrd*^{-/-}). (**f**) Representative FACS plots of CD11b-SiglecF⁺ alveolar macrophages after intratracheal administration of CLL or PBS-L in vehicle-treated and RTX-treated mice 12 h postinfection. Vehicle-treated groups: uninfected ($n = 8$), PBS-L infected ($n = 3$), CLL infected ($n = 3$); RTX-treated groups: uninfected ($n = 8$), PBS-L infected ($n = 4$), CLL infected ($n = 3$). (**g**) Left, survival curves after *S. aureus* lung infection (1×10^8 CFU/mouse) with or without alveolar macrophage depletion. Vehicle + PBS-L ($n = 10$), vehicle + CLL ($n = 10$), RTX + CLL ($n = 10$), RTX + PBS-L ($n = 8$). Log-rank test ($P = 0.37$, RTX + PBS-L versus RTX + CLL; $P = 0.22$, vehicle + PBS-L versus vehicle + CLL). Right, core-body-temperature measurements. Vehicle + PBS-L ($n = 4$), vehicle + CLL, ($n = 4$), RTX + CLL ($n = 4$), and RTX + PBS-L ($n = 4$). Two-way RM ANOVA with Bonferroni post tests. One experiment with multiple biological replicates was performed for **e**, and two independent experiments were performed for **a–d** and **f–g**. Data shown in **a–c**, **e** (core body temperature), and **g** (core body temperature) are mean \pm s.e.m.

not differ in the lungs of RTX-treated *Tcrd*^{-/-} mice and RTX-treated WT mice (**Supplementary Fig. 26**), thus suggesting that $\gamma\delta$ T cells and neutrophils are separately regulated.

We next determined whether alveolar macrophages mediated neuronal regulation of the host defense (**Fig. 5g**). Mice were intratracheally instilled with clodronate-laden liposomes (CLL) to kill alveolar macrophages through phagocytosis-dependent apoptosis. PBS-encapsulated liposomes (PBS-L) were used as a control treatment. CLL treatment specifically eliminated alveolar macrophages (SiglecF⁺ CD11c⁺CD64⁺F4/80⁺) but not interstitial macrophages or dendritic cells (**Fig. 5f** and **Supplementary Fig. 27**). Alveolar-macrophage

depletion did not alter the greater survival or core-body-temperature maintenance of RTX-treated compared with vehicle-treated mice (**Fig. 5g**). Together, our results suggested that the RTX-treatment-mediated enhancement of MRSA immunity requires both $\gamma\delta$ T cells and neutrophils but not alveolar macrophages.

Ablation of vagal TRPV1 neurons improves host defense

The vagus nerve provides the major source of sensory innervation of the lung. The cell bodies of vagal afferents reside in fused ganglia at the base of the skull, controlling coughing, breathing, and bronchoconstriction^{5,6}. Our previous experimental approaches targeted

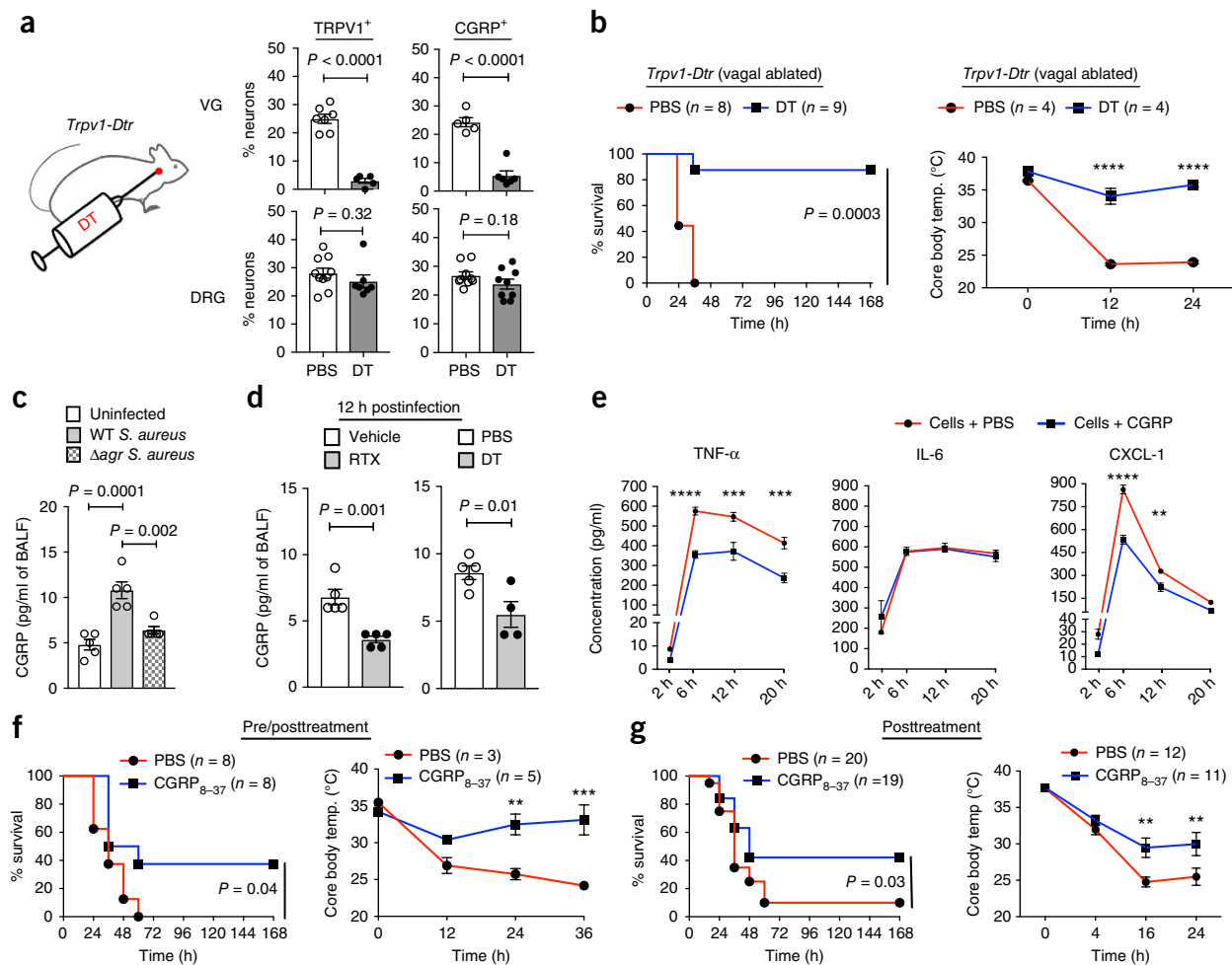


Figure 6 Vagal TRPV1 neurons and the neuropeptide CGRP regulate *S. aureus* pneumonia. **(a)** DT or PBS alone was injected bilaterally into VG in *Trpv1-Dtr* mice. Quantification of proportions of TRPV1⁺ and CGRP⁺ neurons in VG and DRG (T1-T9) of vagal DT-injected mice ($n = 3$) and PBS-injected littermate-control ($n = 3$) mice. Statistical analysis by two-tailed unpaired *t* tests. **(b)** Left, survival curves of PBS VG-injected *Trpv1-Dtr* mice ($n = 9$) compared with DT vagal-injected *Trpv1-Dtr* mice ($n = 8$) after lethal *S. aureus* lung infection (1.3×10^8 to 1.4×10^8 CFU/mouse). Log-rank test, $P = 0.0003$. Right, core body temperature in PBS vagal-injected *Trpv1-Dtr* mice ($n = 4$) compared with DT vagal-injected *Trpv1-Dtr* mice ($n = 4$) after infection. Two-way RM ANOVA with Bonferroni post tests (**** $P < 0.0001$). **(c)** CGRP levels in the BALF in uninfected mice or mice 12 h after infection with WT USA300 *S. aureus* (0.8×10^8 CFU/mouse) or Δagr USA300 *S. aureus* (0.8×10^8 CFU/mouse); uninfected ($n = 5$), WT infected ($n = 5$), and Δagr infected ($n = 5$). Statistical analysis by one-way ANOVA with Bonferroni post tests. **(d)** CGRP levels in the BALF in RTX-treated mice ($n = 5$) and vehicle-treated mice ($n = 5$); or CGRP levels in vagal DT-treated ($n = 5$) or PBS-treated *Trpv1-Dtr* mice ($n = 4$) 12 h after WT *S. aureus* infection (1.1×10^8 to 1.4×10^8 CFU/mouse). Statistical analysis by two-tailed unpaired *t* test. **(e)** Production levels of TNF- α , IL-6, and CXCL-1 by whole lung cell cultures after infection with *S. aureus* at a multiplicity of infection (MOI) of 2 at 2 h, 6 h, 12 h, and 20 h postinfection with or without CGRP α (100 nM). Statistical analysis by two-way ANOVA with Bonferroni post tests. (** $P < 0.01$; *** $P < 0.001$; **** $P < 0.0001$). **(f)** The CGRP-receptor antagonist CGRP₈₋₃₇ was administered systemically (i.p.) at 800 ng (256 pmol) per dose dissolved in PBS, at -24 h, -2 h, 12 h, 24 h, 36 h and 48 h relative to intratracheal *S. aureus* infection (0 h). Control mice received i.p. PBS injections at the same time points. Left, survival curves for mice (PBS treated, $n = 8$; CGRP₈₋₃₇ treated, $n = 8$) after *S. aureus* lung infection. Log-rank test, $P = 0.04$. Right, core-body-temperature measurements (PBS treated, $n = 3$; CGRP₈₋₃₇ treated, $n = 5$) after *S. aureus* infection. Two-way RM ANOVA with Bonferroni post tests (** $P = 0.004$; *** $P = 0.0002$). **(g)** CGRP₈₋₃₇ was administered i.p. at 7.5 μ g (2.4 nmol) per dose in PBS at 4-h, 16-h and 24-h time points relative to intratracheal *S. aureus* infection (0 h). Control mice received i.p. PBS injections at the same time points. Left, survival curves for PBS-treated ($n = 20$) and CGRP₈₋₃₇-treated ($n = 19$) mice. Log-rank test, $P = 0.03$. Right, core body temperature of PBS-treated ($n = 12$) and CGRP₈₋₃₇-treated ($n = 11$) mice. Two-way RM ANOVA with Bonferroni post tests (** $P = 0.002$ (16 h); ** $P = 0.004$ (24 h)). One experiment was performed with multiple biological replicates for **a**, **d**, and **f**; two independent experiments were performed for **b**, **c**, and **e**; three independent experiments were performed for **g**.

all TRPV1⁺ cells, including both DRG and VG neurons. We hypothesized that vagal TRPV1⁺ neurons might include the subset regulating neuroimmunological suppression. To specifically target these neurons, we performed bilateral intraganglionic DT injections into the VG in 5- to 9-week-old *Trpv1-Dtr* mice. Immunostaining showed that vagal but not DRG TRPV1⁺ neurons were specifically ablated (**Fig. 6a**

and **Supplementary Fig. 28**). Vagal TRPV1⁺ neuron ablation did not alter the heart rate, oxygen saturation, perfusion, or respiratory rate (**Supplementary Fig. 6**). Mice were rested 2 weeks after intraganglionic injections, then infected with a lethal dose of MRSA. We observed a striking survival benefit in vagal DT-injected *Trpv1-Dtr* mice compared with vagal PBS-injected mice, and better maintenance of core body

temperature (Fig. 6b). All mice from the PBS-injected group died within 72 h after infection, whereas a 90% survival rate was observed among mice lacking vagal TRPV1 neurons (Fig. 6b). The greater survival in vagal DT-treated mice correlated with higher neutrophil recruitment and lower lung bacterial burdens (Supplementary Fig. 29).

Nociceptive neuropeptide CGRP modulates lung antimicrobial defense

Nociceptor neurons actively communicate with the immune system through their release of neuropeptides stored within peripheral nerve terminals²⁹. The nociceptive neuropeptide CGRP inhibits TNF- α production in macrophages and suppresses lymph node hypertrophy in skin bacterial infection^{29,30}. We hypothesized that CGRP might mediate neuroimmunological signaling during lethal bacterial pneumonia. We found that CGRP levels significantly increased in the BALF after *S. aureus* infection (Fig. 6c). Infection with an *S. aureus* strain mutant for *agr*, a key bicomponent quorum-sensing regulator of virulence-factor expression³¹, did not induce CGRP release into the BALF (Fig. 6c). *S. aureus* also directly induced cultured neuronal release of CGRP *in vitro*, in a manner dependent on *agr* (Supplementary Fig. 30). TRPV1⁺ cells mediated CGRP release in the lungs, because CGRP levels were significantly lower in the BALF in RTX-treated and vagal DT-treated *Trpv1-Dtr* mice than in control-infected mice at 12 h postinfection (Fig. 6d). CGRP levels were also significantly lower in the BALF at steady state in nociceptor-depleted mice than in control nondepleted mice (Supplementary Fig. 31).

We next asked whether CGRP might play a role in MRSA pneumonia. Quantitative PCR analysis showed that lung $\gamma\delta$ T cells and neutrophils expressed *Ramp1* and *Calcr1*, which encode the cognate CGRP receptor (Supplementary Fig. 32). We found that CGRP treatment inhibited lung-cell production of TNF- α and CXCL1, but not IL-6, in response to MRSA infection (Fig. 6e). Increasing concentrations of CGRP also inhibited intracellular killing of *S. aureus* by mouse neutrophils (Supplementary Fig. 33). To explore the involvement of CGRP in host defense, we treated mice with the competitive CGRP peptide antagonist CGRP₈₋₃₇ at time points before and after *S. aureus* lung infection (Fig. 6f). This treatment, compared with vehicle treatment, improved survival and core-body-temperature maintenance (Fig. 6f). We next found that CGRP₈₋₃₇ administered at time points after *S. aureus* infection also significantly improved survival and core-body-temperature maintenance (Fig. 6g). These data showed that nociceptors mediate CGRP release during lung infections and that postinfection blockade of CGRP signaling may aid in treatment of bacterial pneumonia.

DISCUSSION

Nociceptor neurons and immune cells play key roles in protecting organisms from environmental dangers. It is potentially advantageous that interactions between these cell types coordinate host responses to pathogen invasion. We found that TRPV1⁺ afferents in the VG played a critical role in modulating innate immune responses against MRSA lethal pneumonia. Targeting these neurons through *Trpv1-Dtr*-mediated ablation (or RTX treatment) improved survival, neutrophil and $\gamma\delta$ T cell responses, and bacterial clearance. *Nav1.8-cre; Dta* mice, in which an overlapping though distinct nociceptor subset is targeted, showed a milder protective phenotype. Both strategies paradoxically resulted in increased bacterial dissemination. These data suggested that differences in phenotypes (lung clearance versus barrier function) are mediated by distinct neuronal subsets. A recent study has shown that *Trpv1* expression in the adult DRG is mainly restricted to CGRP⁺ and substance P (SP)⁺ C fibers¹⁴. In contrast, Nav1.8 has been found

to be expressed in myelinated A fibers as well as C fibers³². Another study has shown that *Nav1.8-Cre; Dta* mice still possess CGRP⁺ neurons expressing TRPV1 (ref. 21). Therefore, future experiments using more refined genetic tools should help to distinguish the functional contributions of individual TRPV1⁺ and/or Nav1.8⁺ neuronal subsets in pulmonary immunity and barrier function.

Our work adds to recent studies showing major physiological roles for neuroimmunological interactions at peripheral barrier tissues³³. In the respiratory tract, nociceptors actively cross-talk with immune cells, thereby mediating allergic airway inflammation^{5,11,12}. Skin-innervating nociceptors drive inflammation and immunological activation in mouse models of psoriasis²⁰ and contact dermatitis³⁴. In the gut, sympathetic neurons regulate macrophage tissue programming at homeostasis and during *Salmonella* infection³⁵.

We found that nociceptors suppressed pulmonary $\gamma\delta$ T cell- and neutrophil-mediated host defense during MRSA lung infections. A recent study has found that nociceptors drive dendritic-cell IL-23 production and $\gamma\delta$ T cell activation during skin invasion by the fungal pathogen *Candida albicans*¹⁹. The observed phenotypic difference in that study compared with our study is interesting, because differential interactions of vagal versus somatosensory sensory neurons may occur with immune-cell types at different barrier sites. Diverse $\gamma\delta$ T cell populations seed mucosal and epithelial sites²⁷. In the skin, epidermal $\gamma\delta$ T cells are mostly V γ 5⁺ cells that mediate barrier integrity, whereas dermal $\gamma\delta$ T cells do not express V γ 5, but ~40% of them are V γ 4⁺ and are involved primarily in IL-17A production³⁶. IL-17 production by $\gamma\delta$ T cells has also been found to mediate host defense against *S. aureus* skin infections^{28,37}. Heterogeneous subsets of $\gamma\delta$ T cells are found in the respiratory tract, including V γ 1⁺, V γ 2⁺, and V γ 6⁺ populations³⁸.

It is striking that vagal sensory afferents, which comprise fewer than 5,000 neurons, are able to potentially regulate antimicrobial immunity. Distinct vagal afferents control physiological functions including breathing and nutrient sensation^{6,39}. It would be interesting to ascertain how neuronal subsets differentially cross-talk with immune cells. Immune cells may utilize nerves as tracts for migration, as has been observed for dendritic-cell interactions with Nav1.8⁺ nociceptors in the skin²⁰. Lung-resident immune cells may be proximal to vagal nerve afferents and may consequently be able to set up local neuroimmunological responses. Recently, the neuropeptide NMU has been found to drive ILC2-mediated inflammation in the gut and lungs⁴⁰⁻⁴². We found that nociceptors released the neuropeptide CGRP into the airways during infection and downregulated immunity. CGRP has previously been linked to vasodilation and vascular permeability⁴³. CGRP suppresses CXCL1, an important chemokine for lung-neutrophil chemoattraction⁴⁴. Furthermore, CGRP antagonism improves survival outcomes in MRSA-infected mice and is therefore a potential target for clinical application in pneumonia.

Notably, other mechanisms beside CGRP signaling could mediate nociceptor immunological signaling. Nociceptors release glutamate, ATP, and other neuropeptides including SP, neurokinin A, and VIP. They also upregulate cytokines including CCL2 (ref. 45) and CSF-1 after nerve injury⁴⁶. Vagal afferents may also induce sensoriautonomic neuroimmunological reflexes including a 'cholinergic antiinflammatory reflex', which acts through vagal autonomic efferents and downregulates peripheral macrophage TNF- α production⁴⁷.

The role of nociceptors in host defense may vary depending on the type of pathogenic invasion. Whereas increased neutrophil influx confers host protection against MRSA pneumonia, the same responses could lead to immunopathology in other infections. For example, influenza virus and severe acute respiratory syndrome coronavirus

cause pathology through overactivation of lung inflammation^{48,49}. In pneumonia caused by *K. pneumoniae*, *Escherichia coli*, and *S. pneumoniae*, bacterial dissemination is a primary cause of sepsis and mortality^{50,51}. For MRSA-induced pneumonia, lethality is mainly mediated by damage to the lungs by secreted exotoxins (Hla and PVL) rather than bacterial dissemination^{3,52}. These differences in bacterial pathogenesis may explain our observed differences in responses to distinct pathogens in nociceptor-ablated mice.

Our study demonstrates that nociceptors play a critical role in regulating pulmonary immunity and the outcomes of bacterial lung infections. Targeting neuroimmunological communication through CGRP or other molecular mechanisms may be an effective approach to enhance host protection against pneumonia.

METHODS

Methods, including statements of data availability and any associated accession codes and references, are available in the [online version of the paper](#).

Note: Any Supplementary Information and Source Data files are available in the online version of the paper.

ACKNOWLEDGMENTS

We thank K. Blake and N. Lai for technical assistance, and J. Bubeck Wardenburg and C. Altier for helpful discussions. We thank M. Hoon (NIH) for *Trpv1-Dtr* mice, C. Benoist (Harvard Medical School) and A. Mann (Harvard Medical School) for *Tcrd*^{-/-} mice, G. Pier (Brigham and Women's Hospital) and M. Gadjeva (Brigham and Women's Hospital) for *P. aeruginosa*, R. Malley (Boston Children's Hospital) for *S. pneumoniae*, and M. Otto (NIH) for *S. aureus* bacterial strains. This work was supported by National Institutes of Health (NIH) grants DP2AT009499 (I.M.C.), K22AI114810 (I.M.C.), R01AI130019 (I.M.C.), 1KO8AI123516 (P.R.B.), and R01HL132255 (S.D.L.); an HHMI Faculty Scholars Award (S.D.L.); NIH 5F31HL132645 (B.D.U.); and Canadian Institutes of Health Research (CIHR) grant RS-342013 (B.G.Y.).

AUTHOR CONTRIBUTIONS

P.B. and I.M.C. conceived the study. P.B., B.D.U., L.L., B.G.Y., A.W., P.R.B., V.K.K., S.D.L., and I.M.C. designed experiments, analyzed data, and interpreted results. P.B. performed animal infections, survival analysis, bacterial-load recovery, cytokine measurements, FACS, CGRP assays, and neutrophil killing experiments; B.D.U. performed VG injections and immunostaining; A.W. and P.R.B. performed purification of lung cells and quantitative PCR experiments; M.B. performed lung immunostaining and quantification; T.K. and Y.W. performed cytokine measurements and histology; Y.Z. performed neuronal cultures and CGRP assays; L.L. and B.G.Y. performed animal infections with *in vivo* intravital microscopy of neutrophil movement and migration. P.B. and I.M.C. wrote the manuscript, which was edited by S.D.L., B.G.Y., B.D.U., P.B. and I.M.C.

COMPETING INTERESTS

P.B. and I.M.C. are co-inventors on a patent application filed by Harvard incorporating discoveries described in the manuscript.

Reprints and permissions information is available online at <http://www.nature.com/reprints/index.html>. Publisher's note: Springer Nature remains neutral with regard to jurisdictional claims in published maps and institutional affiliations.

- Parker, D. & Prince, A. Immunopathogenesis of *Staphylococcus aureus* pulmonary infection. *Semin. Immunopathol.* **34**, 281–297 (2012).
- Tong, S.Y., Davis, J.S., Eichenberger, E., Holland, T.L. & Fowler, V.G. Jr. *Staphylococcus aureus* infections: epidemiology, pathophysiology, clinical manifestations, and management. *Clin. Microbiol. Rev.* **28**, 603–661 (2015).
- Inoshima, I. *et al.* A *Staphylococcus aureus* pore-forming toxin subverts the activity of ADAM10 to cause lethal infection in mice. *Nat. Med.* **17**, 1310–1314 (2011).
- Mizgerd, J.P. Acute lower respiratory tract infection. *N. Engl. J. Med.* **358**, 716–727 (2008).
- Tränkner, D., Hahne, N., Sugino, K., Hoon, M.A. & Zuker, C. Population of sensory neurons essential for asthmatic hyperreactivity of inflamed airways. *Proc. Natl. Acad. Sci. USA* **111**, 11515–11520 (2014).
- Chang, R.B., Strohlic, D.E., Williams, E.K., Umans, B.D. & Liberles, S.D. Vagal sensory neuron subtypes that differentially control breathing. *Cell* **161**, 622–633 (2015).
- Mazzone, S.B. & Udem, B.J. Vagal afferent innervation of the airways in health and disease. *Physiol. Rev.* **96**, 975–1024 (2016).
- Basbaum, A.I., Bautista, D.M., Scherrer, G. & Julius, D. Cellular and molecular mechanisms of pain. *Cell* **139**, 267–284 (2009).
- Canning, B.J., Mori, N. & Mazzone, S.B. Vagal afferent nerves regulating the cough reflex. *Respir. Physiol. Neurobiol.* **152**, 223–242 (2006).
- Dubin, A.E. & Patapoutian, A. Nociceptors: the sensors of the pain pathway. *J. Clin. Invest.* **120**, 3760–3772 (2010).
- Caceres, A.I. *et al.* A sensory neuronal ion channel essential for airway inflammation and hyperreactivity in asthma. *Proc. Natl. Acad. Sci. USA* **106**, 9099–9104 (2009).
- Talbot, S. *et al.* Silencing nociceptor neurons reduces allergic airway inflammation. *Neuron* **87**, 341–354 (2015).
- Julius, D. TRP channels and pain. *Annu. Rev. Cell Dev. Biol.* **29**, 355–384 (2013).
- Cavanaugh, D.J. *et al.* Restriction of transient receptor potential vanilloid-1 to the peptidergic subset of primary afferent neurons follows its developmental downregulation in nonpeptidergic neurons. *J. Neurosci.* **31**, 10119–10127 (2011).
- Mishra, S.K. & Hoon, M.A. Ablation of TrpV1 neurons reveals their selective role in thermal pain sensation. *Mol. Cell. Neurosci.* **43**, 157–163 (2010).
- Pogorzala, L.A., Mishra, S.K. & Hoon, M.A. The cellular code for mammalian thermosensation. *J. Neurosci.* **33**, 5533–5541 (2013).
- Mishra, S.K., Tisel, S.M., Orestes, P., Bhargoo, S.K. & Hoon, M.A. TRPV1-lineage neurons are required for thermal sensation. *EMBO J.* **30**, 582–593 (2011).
- Kissin, I. & Szallasi, A. Therapeutic targeting of TRPV1 by resiniferatoxin, from preclinical studies to clinical trials. *Curr. Top. Med. Chem.* **11**, 2159–2170 (2011).
- Kashem, S.W. *et al.* Nociceptive sensory fibers drive interleukin-23 production from CD301b+ dermal dendritic cells and drive protective cutaneous immunity. *Immunity* **43**, 515–526 (2015).
- Riol-Blanco, L. *et al.* Nociceptive sensory neurons drive interleukin-23-mediated psoriasisiform skin inflammation. *Nature* **510**, 157–161 (2014).
- Abrahamsen, B. *et al.* The cell and molecular basis of mechanical, cold, and inflammatory pain. *Science* **321**, 702–705 (2008).
- Fernandes, E.S. *et al.* TRPV1 deletion enhances local inflammation and accelerates the onset of systemic inflammatory response syndrome. *J. Immunol.* **188**, 5741–5751 (2012).
- Rigby, K.M. & DeLeo, F.R. Neutrophils in innate host defense against *Staphylococcus aureus* infections. *Semin. Immunopathol.* **34**, 237–259 (2012).
- Yipp, B.G. *et al.* The lung is a host defense niche for immediate neutrophil-mediated vascular protection. *Sci. Immunol.* **2**, eaam8929 (2017).
- Yipp, B.G. *et al.* Infection-induced NETosis is a dynamic process involving neutrophil multitasking in vivo. *Nat. Med.* **18**, 1386–1393 (2012).
- Su, A.I. *et al.* A gene atlas of the mouse and human protein-encoding transcriptomes. *Proc. Natl. Acad. Sci. USA* **101**, 6062–6067 (2004).
- Zheng, J., Liu, Y., Lau, Y.L. & Tu, W. $\gamma\delta$ -T cells: an unpolished sword in human anti-infection immunity. *Cell. Mol. Immunol.* **10**, 50–57 (2013).
- Murphy, A.G. *et al.* *Staphylococcus aureus* infection of mice expands a population of memory $\gamma\delta$ T cells that are protective against subsequent infection. *J. Immunol.* **192**, 3697–3708 (2014).
- Pinho-Ribeiro, F.A., Verri, W.A. Jr. & Chiu, I.M. Nociceptor sensory neuron-immune interactions in pain and inflammation. *Trends Immunol.* **38**, 5–19 (2017).
- Chiu, I.M. *et al.* Bacteria activate sensory neurons that modulate pain and inflammation. *Nature* **501**, 52–57 (2013).
- Cheung, G.Y., Wang, R., Khan, B.A., Sturdevant, D.E. & Otto, M. Role of the accessory gene regulator agr in community-associated methicillin-resistant *Staphylococcus aureus* pathogenesis. *Infect. Immun.* **79**, 1927–1935 (2011).
- Shields, S.D. *et al.* Nav1.8 expression is not restricted to nociceptors in mouse peripheral nervous system. *Pain* **153**, 2017–2030 (2012).
- Veiga-Fernandes, H. & Mucida, D. Neuro-immune interactions at barrier surfaces. *Cell* **165**, 801–811 (2016).
- Liu, B. *et al.* IL-33/ST2 signaling excites sensory neurons and mediates itch response in a mouse model of poison ivy contact allergy. *Proc. Natl. Acad. Sci. USA* **113**, E7572–E7579 (2016).
- Gabanyi, I. *et al.* Neuro-immune interactions drive tissue programming in intestinal macrophages. *Cell* **164**, 378–391 (2016).
- Tay, S.S., Roediger, B., Tong, P.L., Tikoo, S. & Weninger, W. The skin-resident immune network. *Curr. Dermatol. Rep.* **3**, 13–22 (2013).
- Cho, J.S. *et al.* IL-17 is essential for host defense against cutaneous *Staphylococcus aureus* infection in mice. *J. Clin. Invest.* **120**, 1762–1773 (2010).
- Cheng, M. & Hu, S. Lung-resident $\gamma\delta$ T cells and their roles in lung diseases. *Immunology* **151**, 375–384 (2017).
- Williams, E.K. *et al.* Sensory neurons that detect stretch and nutrients in the digestive system. *Cell* **166**, 209–221 (2016).
- Cardoso, V. *et al.* Neuronal regulation of type 2 innate lymphoid cells via neuromedin U. *Nature* **549**, 277–281 (2017).

41. Klose, C.S.N. *et al.* The neuropeptide neuromedin U stimulates innate lymphoid cells and type 2 inflammation. *Nature* **549**, 282–286 (2017).
42. Wallrapp, A. *et al.* The neuropeptide NMU amplifies ILC2-driven allergic lung inflammation. *Nature* **549**, 351–356 (2017).
43. Franco-Cereceda, A. *et al.* Cardiovascular effects of calcitonin gene-related peptides I and II in man. *Circ. Res.* **60**, 393–397 (1987).
44. Sawant, K.V. *et al.* Chemokine CXCL1-mediated neutrophil trafficking in the lung: role of CXCR2 activation. *J. Innate Immun.* **7**, 647–658 (2015).
45. Kwon, M.J. *et al.* CCL2 mediates neuron-macrophage interactions to drive proregenerative macrophage activation following preconditioning injury. *J. Neurosci.* **35**, 15934–15947 (2015).
46. Guan, Z. *et al.* Injured sensory neuron-derived CSF1 induces microglial proliferation and DAP12-dependent pain. *Nat. Neurosci.* **19**, 94–101 (2016).
47. Pavlov, V.A. *et al.* Brain acetylcholinesterase activity controls systemic cytokine levels through the cholinergic anti-inflammatory pathway. *Brain Behav. Immun.* **23**, 41–45 (2009).
48. de Jong, M.D. *et al.* Fatal outcome of human influenza A (H5N1) is associated with high viral load and hypercytokinemia. *Nat. Med.* **12**, 1203–1207 (2006).
49. Tisoncik, J.R. *et al.* Into the eye of the cytokine storm. *Microbiol. Mol. Biol. Rev.* **76**, 16–32 (2012).
50. Hommes, T.J. *et al.* DNAX-activating protein of 12 kDa impairs host defense in pneumococcal pneumonia. *Crit. Care Med.* **42**, e783–e790 (2014).
51. Xiong, H. *et al.* Innate lymphocyte/Ly6Chi monocyte crosstalk promotes *Klebsiella Pneumoniae* clearance. *Cell* **165**, 679–689 (2016).
52. Labandeira-Rey, M. *et al.* *Staphylococcus aureus* Panton-Valentine leukocidin causes necrotizing pneumonia. *Science* **315**, 1130–1133 (2007).

ONLINE METHODS

Mice. All animal experiments were approved by the Harvard Medical School Institutional Animal Care and Use Committee (IACUC) or by the University of Calgary Animal Care Committee. Mice were housed in a specific-pathogen-free animal facility at Harvard Medical School or the University of Calgary. C57BL/6J, B6.Trpv1^{-/-}, B6.Tcrd^{-/-}, B6.Dta^{+/+}, and B6129.Trpa1^{-/-} mice were purchased from Jackson Laboratories. Trpv1-Dtr mice¹⁶ were provided by M. Hoon (NIH). Nav1.8-cre mice²¹ were originally from J. Wood (University College London). Nav1.8-cre^{+/-} mice were bred with B6.Dta^{+/+} mice to generate Nav1.8-cre^{+/-}; Dta mice and control littermates (Nav1.8-cre^{-/-}; Dta). For Trpv1 and Trpa1 experiments, heterozygous mice were bred to produce WT, heterozygous, and knockout littermates. Age-matched 8- to 14-week-old male and female mice were used for experiments.

Bacterial strains and cultures. The MRSA strain USA300/LAC⁵³ was provided by M. Otto (NIH). For infection, USA300/LAC was grown overnight (O/N) at 37 °C in tryptic soy broth (TSB, Sigma) at 250 r.p.m. and was subcultured at a 1:100 dilution for 3.5 h in TSB to mid-log phase. *K. pneumoniae* strain 43816 serotype 2 was purchased from American Type Culture Collection and was grown O/N at 37 °C in TSB at 250 r.p.m. for infection. *S. pneumoniae* WU-2 strain from R. Malley (Boston Children's Hospital) was grown at 37 °C under 5% CO₂ without shaking for 18 h in Todd's Hewitt broth (THB, Sigma) with 0.5% yeast extract and was subcultured at a 1:10 dilution for 8 h in fresh THB with 0.5% yeast extract to reach mid-log phase for infection. *P. aeruginosa* strain PA01V from G. Pier (Brigham and Women's Hospital) was grown O/N at 37 °C in TSB at 250 r.p.m. and was subcultured at a 1:100 dilution for 4 h in TSB for infection. For all strains, cultures were centrifuged at 5,000 r.p.m. for 5 min, and bacterial pellets were washed and resuspended in phosphate-buffered saline (PBS). The OD₆₀₀ was measured to estimate bacterial density, and serial plating was performed on tryptic soy agar (TSA) plates to quantify CFU values. For intravital imaging, a GFP-MRSA *S. aureus* transgenic bacterium was used, whose construction has been previously reported²⁵.

Bacterial lung infections. For all bacterial infections, age-matched 8- to 14-week-old male and female mice, weighing between 19 and 30 g, were studied. For lethal infections, 50 µl containing 0.8 × 10⁸ to 1.6 × 10⁸ CFU *S. aureus* in PBS was intratracheally inoculated per mouse. Control animals were intratracheally infused with 50 µl PBS only. For sublethal infections, 2 × 10⁷ to 4 × 10⁷ CFU of *S. aureus* was used per mouse. For *S. pneumoniae* infections, 10⁶ CFU in 50 µl PBS was intratracheally inoculated. For *K. pneumoniae* infections, 10⁴ CFU in 50 µl PBS was intratracheally inoculated. For *P. aeruginosa* infections, 7 × 10⁶ CFU in 50 µl PBS was intratracheally inoculated. Mice were monitored twice daily for morbidity and mortality. In some experiments, CGRP₈₋₃₇ (Genscript) was administered i.p. at 800 ng (256 pmol) or 7.5 µg (2.4 nmol) per dose in 200 µl PBS, at different time points relative to infection (0 h). Control mice received 200 µl PBS only.

Vital-sign measurements. Heart rate, oxygen saturation, and perfusion were measured under isoflurane anesthesia by Pulse Oximetry with the Kent Scientific PhysioSuite (Kent Scientific Corporation). For accuracy, measurements were performed three independent times on different days for the same mice, and values represent the average of three measurements. Pulse oximetry could not be used on MRSA-infected mice because they could not survive isoflurane anesthesia, and thus the measurements were performed only at steady state. Respiratory rates were determined by manually recording the number of breaths per minute and were averaged over three measurements. Core body temperature was measured with a rectal thermal probe (Bioseb).

Genetic and chemical ablation of TRPV1⁺ nociceptors. Trpv1-Dtr mice were treated with DT as previously described⁵. Mice were injected i.p. with 200 µg of DT (Sigma Aldrich) dissolved in 100 µl PBS or with 100 µl PBS (vehicle) daily for a 21-d period. 5- to 7-week-old male and female mice were used for these experiments. For chemical ablation of TRPV1⁺ neurons, C57BL/6 mice 4 weeks of age were treated with RTX (Sigma) as previously described^{19,20}. Mice were injected subcutaneously in the flank on consecutive days with

three increasing doses of RTX (30, 70, and 100 µg/kg) dissolved in 2% DMSO with 0.15% Tween 80 in PBS. Control mice were treated with vehicle alone. For intravital imaging experiments, the same dosage for RTX treatment was used in 4-week-old mice, except the vehicle for dissolution was DMSO (without Tween 80). RTX was diluted into DMSO (1 µg/µl) and subsequently into saline before injections. For VG-targeted ablation, we performed bilateral intraganglionic injections of DT or PBS into Trpv1-Dtr mice as previously described⁵. 20 ng DT in 120 nl PBS containing 0.05% Fast Green was injected into nodose/jugular/petrosal VG with a nanoinjector (Drummond Scientific Company). Mice were anesthetized with 1–3% isoflurane with oxygen. The vagal ganglion was exposed after a midline incision in the neck (~1.5 cm in length). DT was gently injected; this process was repeated for the vagal ganglion on the other side of the body.

Bronchoalveolar lavage fluid (BALF) analysis. Mice were euthanized by CO₂ inhalation, and the trachea were exposed and cannulated with a 20-gauge catheter (BD Insyte Autoguard). BALF was collected two times by instilling 0.8 ml of cold PBS containing heparin and dextrose, then centrifuged at 4,000 r.p.m. for 7 min at 4 °C, and the cell pellet was separated from the supernatant. Total BALF leukocytes were counted after red-blood-cell lysis (RBC lysis buffer, eBioscience) and subjected to flow cytometry. Cell-free BALF supernatant was filtered through a 0.22-µm filter and mixed with protease/phosphatase-inhibitor cocktail, then kept at -80 °C for protein and cytokine analysis.

Bacterial-load and cytokine measurements. Lungs and spleen tissues were homogenized in 1 ml sterile water with BB beads (Daisy Outdoor Products) in a Tissue Lyzer II (Qiagen). Lung, spleen homogenates, blood, or BALF was serially diluted in PBS and plated on TSA plates. The bacterial CFU were enumerated after overnight incubation of TSA plates at 37 °C. Cytokine levels in lung homogenates and BALF were measured through enzyme-linked immunosorbent assay (ELISA) kits according to the manufacturer's instructions (Biolegend).

Behavior tests. For behavioral assays, observers were blinded to the treatment group and genotype. To measure heat sensitivity, mice were placed on a hot plate set at 52 °C (IITC Life Science). Latency to hindpaw lifting, licking or flinching was recorded, and stopped at a maximum of 60 s. For tail-flick assays, mice were kept vertically in a relaxed fashion with their tails immersed in a temperature-controlled water bath maintained at 52 °C. The latency to a tail flick was recorded, with a maximum of 60 s.

Immune-cell depletion. For neutrophil depletion, we followed an established protocol⁵⁴. Mice were injected i.p. with 125 µg of anti-GR1 (clone RB6-8C5, BioXCell, NH) (in 200 µl) per mouse 24 h before lung infection. Control mice received 125 µg of rat IgG (Jackson Immunoresearch). For depletion of alveolar macrophages, 100 µl CLL (purchased from <http://clodronateliposomes.org/>) was delivered intratracheally into mice 2 d before infection. Control mice received an equal volume of PBS-L.

Lung-barrier permeability assay. FITC-dextran (Mol Wt 4,000, Sigma) was intratracheally inoculated in 50 µl/mouse at 20 mg per kg body weight. Control mice were inoculated with PBS. Four hours later, mice were euthanized, and blood was collected by cardiac puncture. Blood was allowed to coagulate for 30 min at room temperature in the dark and centrifuged at 2,500g for 15 min. Fluorescence in serum was recorded with a plate reader (BioTek Synergy) and normalized to FITC-dextran standards (1.56–100 µg/ml).

Flow cytometry. Lung tissues were mechanically separated and minced, then digested in DMEM (Life Technologies) containing 2% FBS and 1.5 mg/ml collagenase D (Roche) at 37 °C for 1 h at 250 r.p.m. The cell mixture was passed through an 18-gauge needle three times and filtered through a 70-µm cell strainer (BD). Red blood cells were lysed with RBC lysis buffer (eBioscience), treated with Fc Block (Biolegend), and resuspended in FACS buffer (PBS, 2% FBS, and 1 mM EDTA). For splenocytes, spleens were mashed and filtered through a 70-µm strainer (BD). Red blood cells were lysed with RBC lysis

buffer (eBioscience), treated with Fc Block, and resuspended in FACS buffer. Incubations with antibody cocktails were conducted on ice for 30 min, and samples were subjected to two washes and resuspension in PBS with 2% PFA and 1 mM EDTA before flow cytometry. Antibodies used for staining included: anti-CD11b-Brilliant Violet 605 (clone M1/17, BioLegend), anti-CD45-APC/Cy7 (30-F11, BioLegend), anti-Ly-6G-Alexa Fluor 488 (1A8, BioLegend), anti-Ly-6C-PerCP/Cy5.5 (HK1.4, BioLegend), anti-Gr1-FITC (RB6-8C5, BioLegend), anti-CD4 Pac Blue (GK1.5, BioLegend), anti-CD8 α -PE/Cy7 (53-6.7, BioLegend), anti-CD11c-APC (N418, BioLegend), anti-CD64-Brilliant Violet 421 (X54-5/7.1, BioLegend), anti-SiglecF-Alexa Fluor 488 (E50-2440, BD Bioscience), anti-CD103 PE (2E7, BioLegend), anti-TCR $\gamma\delta$ -PE (GL3, BioLegend), anti-F4/80-FITC (BM8, BioLegend), anti-NK1.1-PerCP/Cy5.5 (NK-1.1, BioLegend), anti-B220-APC (RA3-6B2, BioLegend), anti-CD3 α -PE/Cy7 (17A2, BioLegend), anti-CD24 Brilliant Violet 510 (M1/69, BioLegend), anti-TCR- β Brilliant Violet 421 (H57-597, BioLegend), anti-TCR V γ 1.1-APC (2.11, BioLegend), and anti-TCR V γ 2-PE-Cy7 (UC3-10A6, eBioscience). Flow cytometry was conducted on an LSRII flow cytometer (BD). Data were collected with BD DIVA software, and files were analyzed with FlowJo (Treestar, version 10.0.8r1). A live-cell stain (eFluor 450, eBioscience) was used to exclude dead cells. Positive staining and gates for each fluorescent marker were defined by comparing full stain sets with fluorescence minus one (FMO) control stain sets.

Fluorescence-activated cell sorting of lung immune cells. For FACS purification of lung-resident populations, we used antibodies against CD3 ϵ (clone 145-2C11), CD4 (clone RM4-5), CD11b (clone M1/70), Ly6G (clone 1A8), CD19 (clone 6D5), CD45 (clone 30-F11), TCR β (clone H57-597), and TCR $\gamma\delta$ (clone GL3) from BioLegend. 7AAD was from BD Pharmingen. Single-cell suspensions were generated from lungs of two or three C57Bl/6J mice with a lung-dissociation kit (Miltenyi Biotec). Single-cell suspensions were incubated with CD90.2 MicroBeads (Miltenyi Biotec) and separated into CD90.2-positive and CD90.2-negative fractions. Both fractions were stained on ice with surface antibodies and live/dead marker 7AAD, and sorted on a BD FACSAria (BD Biosciences). Different cell types were identified through the following gating strategies: B cells (7AAD⁻CD45⁺CD19⁺) and neutrophils (7AAD⁻CD45⁺CD11b⁺Ly6G⁺) were sorted from the preenriched CD90.2⁻ cell fraction, whereas CD4⁺ T cells (7AAD⁻CD45⁺CD3⁺TCR β ⁺CD4⁺) and TCR $\gamma\delta$ T cells (7AAD⁻CD45⁺CD3⁺TCR β ⁻TCR $\gamma\delta$ ⁺) were sorted from the preenriched CD90.2⁺ cell fraction.

Quantitative real-time PCR. An RNeasy Plus Mini Kit (Qiagen) was used to isolate RNA, which was reverse transcribed to cDNA with an iScript cDNA Synthesis Kit (Bio-Rad). Relative gene expression was determined by quantitative real-time PCR on a ViiA7 System (Thermo Fisher Scientific) with TaqMan Fast Advanced Master Mix (Thermo Fisher Scientific) with the following primer/probe sets: *Trpv1* (Mm01246300_m1), *Ramp1* (Mm00489796_m1), *Calcr1* (Mm00516986_m1), and *Actb* (Applied Biosystems). Expression values relative to *Actb* (detected in the same sample by duplex qPCR) were calculated.

Neuronal cultures and CGRP analysis. DRG neuron cultures were grown as previously described³⁰. In brief, total DRG were dissected from 8- to 12-week-old mice and digested in HEPES-buffered saline (Sigma) containing 1 mg/ml collagenase A and 3 mg/ml dispase II (Roche Applied Sciences) for 60 min at 37 °C. The cell suspension was triturated with fire-polished Pasteur pipettes, then centrifuged over a 12% BSA (Sigma) gradient. The top layer of debris was discarded, and cell pellets were resuspended in neurobasal (NB) medium containing B27 (Life Technologies). Neurons were plated on laminin-coated 96-well culture dishes in NB medium containing B27, 50 ng/ml nerve growth factor (Life Technologies), and penicillin/streptomycin (Life Technologies). The medium was changed every other day. At day 7, DRG neurons were stimulated with *S. aureus* or 500 nM capsaicin (Sigma) for 30 min, and supernatant was collected. CGRP levels in the culture supernatant, BALF, or lung homogenates were determined with a CGRP EIA kit according to the manufacturer's instructions (Cayman Chemical).

Gene expression analysis. We analyzed transcript levels in mouse transcriptome data sets deposited at the Immunological Genome Project⁵⁵ (GEO GSE15907).

Data sets for CD4⁺, CD8⁺ T cells, B cells, $\gamma\delta$ T cells, NK cells, macrophages, dendritic cells, and neutrophils were analyzed. *Trpv1* expression was also analyzed in the Mouse Gene Atlas MOE430 transcriptome data set²⁶ (GEO GSE1133). Microarray data were background corrected and normalized with the robust multiarray average (RMA) algorithm in GenePattern (Broad Institute). A heat map for average transcript values was plotted with Morpheus (Broad Institute), *Trpv1* levels were also plotted with Prism (GraphPad).

Lung histology. Whole lungs were dissected from mice after euthanasia, fixed and stored in 10% formalin (Sigma Aldrich). Samples were embedded, sectioned, and stained with H&E or with a Brown and Brenn stain for Gram-positive bacteria by the Harvard Rodent Histopathology Core. Light microscopy of histological sections was conducted on a Nikon Ti-E microscope.

Immunofluorescence and microscopy. For immunostaining, mice were perfused with PBS followed by 4% paraformaldehyde (PFA) in PBS. VG and thoracic DRG (T1-T13) were dissected and postfixed for 2 h in 4% PFA/PBS at 4 °C, incubated O/N at 4 °C with 30% sucrose/PBS, embedded in optimal cutting temperature compound (OCT, Tissue-Tek, PA) and stored at -80 °C. 12- μ m cryosections were cut and immunostained with the following antibodies: guinea pig anti-TRPV1 (Millipore, AB5566, dilution 1:1,000), rabbit anti-CGRP (Sigma, C8198, dilution 1:5,000), mouse anti-NF-200 (Millipore, MAB5266, dilution 1:1,000), rabbit anti- β III-tubulin (Tuj1) (Abcam, ab18207, dilution 1:1,000), and mouse anti- β III-tubulin (Abcam, ab7751, dilution 1:500). Secondary antibodies included DyLight-488 donkey anti-rabbit IgG (Abcam, 1:500), CF-488A goat anti-guinea pig IgG (Sigma, 1:500), Alexa 488 donkey anti-mouse IgG (Abcam, 1:500), Alexa 594 donkey anti-mouse IgG (Abcam, 1:500) and Alexa 594 donkey anti-rabbit IgG (Abcam, 1:500). Sections were mounted in Vectashield and imaged with a Nikon Ti-E microscope with 10 \times magnification with NIS Elements software (Nikon, version AR3.22.08). For quantification of VG and DRG neuronal populations, images were analyzed by observers blinded to genotypes and treatment groups. β -tubulin-III was used as a general neuronal marker. Multiple fields were captured from three mice per group.

For immunostaining of lung sections, lungs were perfused with cold PBS and gravity inflated with 4% PFA/PBS. After overnight fixation at 4 °C, lungs were incubated 2 d in 30% sucrose/PBS, cryoembedded in OCT, and stored at -80 °C until sectioning. 40- μ m cryosections were blocked for 4 h in PBS with 10% donkey serum, 2% bovine serum albumin (BSA), and 0.8% Triton X-100. Sections were incubated with rabbit anti-CGRP (C8198, Sigma) at a 1:5,000 dilution in blocking solution (PBS with 2% donkey serum, 2% BSA, and 0.3% Triton X-100) for 16–18 h at 4 °C, then incubated with secondary antibody (Alexa 594 donkey anti-rabbit IgG H&L, Abcam, ab150076) at a 1:500 dilution in blocking solution at 4 °C. Stained specimens were imaged on an inverted laser scanning confocal microscope (Olympus Fluoview FV1000).

Adobe Photoshop (Adobe) was used to quantify CGRP⁺ airway innervation in lung sections. The lasso tool was used to trace the circumference of each inner lung airway on the basis of DAPI staining; The area enclosed (in pixels) was derived from the histogram tool. The traced circumference was expanded by 162 pixels (100 μ m) for each airway. The magic-wand tool was used to select the CGRP⁺ pixels within the circumscribed area and quantified out of the entire airway border, which is the percentage area covered by CGRP⁺ nerve fibers.

Neutrophil isolation and bacterial killing. Mouse bone marrow neutrophils were isolated with an EasySep Mouse Neutrophil Enrichment Kit according to the manufacturer's instructions (StemCell Technologies). A Diff-Quick Stain kit (Thermo scientific) was used to confirm purity, which was found to be >95% neutrophils. To perform bacterial killing assays, 2.5 \times 10⁵ neutrophils were cocultured with 5 \times 10⁵ CFU of *S. aureus* (MOI of 2) in DMEM (Gibco) containing 5% FBS. CGRP (Genescript) was added at different concentrations, and cells were incubated at 37 °C for the indicated times. Neutrophils were then centrifuged at 600 r.p.m. for 2 min, and the pellet was washed twice with PBS and incubated for 30 min with 200 μ g/ml gentamicin. Neutrophils were lysed with 0.1% Triton X-100, and dilutions were plated onto TSA plates to measure intracellular, viable bacteria. Lung cells were also isolated from C57Bl/6J mice

as described above in the flow cytometry section and cocultured with *S. aureus* (MOI of 2) with or without CGRP (100 nM) at the indicated time points for measurement of IL-6, TNF- α , and CXCL-1 levels in culture supernatants with specific ELISA kits (BioLegend).

Pulmonary intravital microscopy. After mice were anesthetized (ketamine, 100 mg/kg; xylazine, 10 mg/kg), they received a jugular vein catheter for administration of fluorescent antibodies or additional anesthetics. To visualize neutrophils and endothelium, 3.5 μ g Alexa Fluor 594-conjugated anti-Ly6G antibody (clone 1A8, BioLegend) and 5 μ g Alexa Fluor 647-conjugated anti-CD31 antibody (clone MEC13.3, BioLegend) were injected intravenously. Mice were placed on a heating pad maintained at 37 °C and connected to mechanical ventilation (Harvard Apparatus) after tracheostomy was performed. Mice were kept in a right lateral decubitus position, and the left lung was exposed after thoracotomy and rib resection. A portion of the lung was immobilized via a gentle vacuum chamber with a glass slide fitted on top. A resonant-scanner confocal microscope (Leica SP8) equipped with a white-light laser and three HyD spectral detectors and a 25 \times /0.9 water objective lens were used for intravital microscopy. Images were acquired every 10 s for a total of 10 min, and three to five fields of view were observed. All videos and images were processed and analyzed with Leica software and Volocity software. For neutrophil behavior analysis, tethering was defined as rapid movement with blood flow and stop for less than 30s. Adhesion was defined as neutrophils that remained stationary for 30 s or longer. Crawling was defined as polarized cells that maintained continuous contact with the endothelium while changing physical location for at least 30 s. Random neutrophils were tracked manually in 10-min videos in Volocity software.

Sample size and statistical analysis. For survival studies, we used animal numbers between 5 and 20 mice per experimental group/genotype. For core-body-temperature measurements, we used animal numbers between 3 and 5 mice per group/genotype. For survival studies and core-body-temperature measurements, experiments were performed at least twice, and data from individual mice were pooled from all experiments. For bacterial-load recovery and FACS analyses, 4–18 mice per group/genotype were used. For measurement of cytokine and CGRP levels, 3–12 mice per group/genotype were used. Survival data were analyzed with the log-rank test; bacterial-load recovery, behavioral data, core body temperature, FACS and cytokines were compared with two-way ANOVA with Bonferroni post tests, one-way ANOVA with Bonferroni post tests, two-tailed unpaired *t* tests for parametric analyses, or Mann–Whitney test for nonparametric analyses. Data were plotted in Prism (GraphPad).

Life Sciences Reporting Summary. Further information on experimental design is available in the **Life Sciences Reporting Summary**.

Data availability. All relevant data are readily available upon reasonable request to the corresponding author.

53. Wang, R. *et al.* Identification of novel cytolytic peptides as key virulence determinants for community-associated MRSA. *Nat. Med.* **13**, 1510–1514 (2007).
54. Ghasemlou, N., Chiu, I.M., Julien, J.P. & Woolf, C.J. CD11b+Ly6G- myeloid cells mediate mechanical inflammatory pain hypersensitivity. *Proc. Natl. Acad. Sci. USA* **112**, E6808–E6817 (2015).
55. Heng, T.S., Painter, M.W. & The Immunological Genome Project Consortium. The Immunological Genome Project: networks of gene expression in immune cells. *Nat. Immunol.* **9**, 1091–1094 (2008).

Life Sciences Reporting Summary

Nature Research wishes to improve the reproducibility of the work that we publish. This form is intended for publication with all accepted life science papers and provides structure for consistency and transparency in reporting. Every life science submission will use this form; some list items might not apply to an individual manuscript, but all fields must be completed for clarity.

For further information on the points included in this form, see [Reporting Life Sciences Research](#). For further information on Nature Research policies, including our [data availability policy](#), see [Authors & Referees](#) and the [Editorial Policy Checklist](#).

► Experimental design

1. Sample size

Describe how sample size was determined.

For lung infection studies and behavioral studies in mice, the numbers of animals were chosen based on the power analyses of past or present studies in the field. For survival studies, we used animal numbers between 5-20 mice per experimental group/genotype. For core body temperature measurements, we used animal numbers between 3-5 mice per experimental group/genotype. For bacterial load recovery measurements and FACS analysis, 4-18 mice per experimental group/genotype was used. For measurement of total protein, cytokine, and CGRP levels in tissue samples, 3-12 mice per group/genotype were used. For in vitro experiments, three or four biological replicates per condition or treatment group were collected for analysis.

2. Data exclusions

Describe any data exclusions.

No data were excluded.

3. Replication

Describe whether the experimental findings were reliably reproduced.

For all lethal and sub-lethal lung bacterial infections, experiments were performed at least twice, and data from individual mice were pooled from all experiments. Similar numbers of mice were used in each experiment in parallel for control and treatment experimental groups. Differences between control and treatment groups or differences between genotypes showed consistent and reproducible results across our study. For in vitro experiments, multiple biological replicates were used for each treatment group. Multiple biological replicates of lung immune cells were purified and sensory ganglia dissected for gene expression analysis. The exact number of independent experiments conducted for each experiment are described in Figure legends.

4. Randomization

Describe how samples/organisms/participants were allocated into experimental groups.

Experiments involving knockout or transgenic mice were carried out across littermates of mixed genotypes (e.g. heterozygous, wild-type or knockout mice) in the same cage that were randomly put together at weaning prior to genotyping. All experiments involving treatments (e.g. RTX vs. vehicle) were performed on equal groups of cagemates or littermates. For infections, the same inoculum of *S. aureus*, *P. aeruginosa*, *K. pneumoniae*, or *S. pneumoniae* and used to infect across experimental groups in random order to ensure equivalent dosing.

5. Blinding

Describe whether the investigators were blinded to group allocation during data collection and/or analysis.

For all lethal and sub-lethal lung bacterial infection experiments in mice, the experimenter measuring survival, temperature, and other parameters was blinded to mouse genotype and treatment groups during infections and post-infection procedures until being unblinded at the analysis stage.

Note: all studies involving animals and/or human research participants must disclose whether blinding and randomization were used.

6. Statistical parameters

For all figures and tables that use statistical methods, confirm that the following items are present in relevant figure legends (or in the Methods section if additional space is needed).

- n/a Confirmed
- The exact sample size (n) for each experimental group/condition, given as a discrete number and unit of measurement (animals, litters, cultures, etc.)
 - A description of how samples were collected, noting whether measurements were taken from distinct samples or whether the same sample was measured repeatedly
 - A statement indicating how many times each experiment was replicated
 - The statistical test(s) used and whether they are one- or two-sided (note: only common tests should be described solely by name; more complex techniques should be described in the Methods section)
 - A description of any assumptions or corrections, such as an adjustment for multiple comparisons
 - The test results (e.g. P values) given as exact values whenever possible and with confidence intervals noted
 - A clear description of statistics including central tendency (e.g. median, mean) and variation (e.g. standard deviation, interquartile range)
 - Clearly defined error bars

See the web collection on [statistics for biologists](#) for further resources and guidance.

► Software

Policy information about [availability of computer code](#)

7. Software

Describe the software used to analyze the data in this study.

Graphpad Prism software (version 7.0B) was used for statistical analyses of survival data, core body temperature data, bacterial load recovery data, total protein/cytokine/CGRP measurements, percentage of cells analyzed by FACS, gene expression data, and neutrophil lung surveillance/movement data. All recordings of intravital microscopy videos were processed and analyzed using Leica software and Volocity software (Perkin Elmer). For neutrophil behavior analysis, random neutrophils were tracked manually in 10-min videos by using Volocity software (Perkin Elmer). FlowJo software (Treestar, version 10.0.8r1) was used for all analyses of flow cytometry data. Immunofluorescence and H&E images were collected using Nikon's NIS Elements software (Nikon, version AR3.22.08). Microarray data from GEO datasets (Accession number GSE15907 and GSE1133) was background corrected and normalized using Robust Multi-array Average (RMA) algorithm in the GenePattern software (Broad Institute). A heatmap for average transcript values was plotted using Morpheus software (Broad Institute). Normalized Trpv1 expression levels were plotted using Prism software (Graphpad). Adobe Photoshop (Adobe) was used to quantify CGRP+ nerve staining in lung section images as described in the Methods section. Prism software (Graphpad) was used to plot Kaplan-Meier survival curves, bar graphs, scatter dot plots, and line graphs presented throughout the manuscript. Adobe Illustrator software (Adobe) was used to generate figures in the manuscript.

For manuscripts utilizing custom algorithms or software that are central to the paper but not yet described in the published literature, software must be made available to editors and reviewers upon request. We strongly encourage code deposition in a community repository (e.g. GitHub). [Nature Methods guidance for providing algorithms and software for publication](#) provides further information on this topic.

► Materials and reagents

Policy information about [availability of materials](#)

8. Materials availability

Indicate whether there are restrictions on availability of unique materials or if these materials are only available for distribution by a for-profit company.

All bacterial strains, mouse strains and reagents used in the study are either commercially available or will be made readily available with no more restrictive terms than a uniform biological materials transfer agreement (UBMTA). We were generously supplied certain reagents for our study through such agreements, including Trpv1-Dtr mice from Mark Hoon (NIH) and MRSA strain USA300 from Mike Otto (NIH).

9. Antibodies

Describe the antibodies used and how they were validated for use in the system under study (i.e. assay and species).

Primary antibodies used for immunostaining are: Guinea pig anti-TRPV1 (Millipore, cat# AB5566): validated by Rat DRG immunostaining (Millipore), in 9 papers including Amadesi et al, *J Comp Neurol* 516:141-56 (2009); We validated its specificity by loss in DRG from TRPV1-DTR neuron ablated mice. Rabbit anti-CGRP (Sigma, cat# C8198): validated by immunostaining of rat DRG by Sigma, in 58 papers including Lorenzo et al, *J Neuroscience* 2014 34:34. Mouse anti NF-200 (Millipore, cat# MAB5266): validated by immunostaining of rat hippocampus (Millipore), in 13 papers including Blanchard et al, *Nature Neuroscience* 18:25-35 (2015). Rabbit anti- β III-tubulin (Abcam, cat# ab18207): validated by immunostaining of cerebellum and western blots (Abcam), in 112 papers including Choi et al, *PLoS One* 12:e0176153 (2017). Mouse anti- β III-tubulin (Abcam, cat# ab7751): validated by immunostaining of Neuro-2a cells (Abcam), in 67 papers including Mao et al, *J Neuroinflammation* 13:308 (2016). Secondary antibodies used for immunostaining are: DyLight-488 Donkey anti-rabbit IgG (Abcam, cat# ab98488): validated by immunostaining of mouse ES cell embryoid bodies (Abcam). CF-488A Goat anti-guinea pig IgG (Sigma, cat# SAB4600040): Validated by immunostaining of HeLa Cells (Sigma). Alexa 594 Donkey anti-mouse IgG (Abcam, cat# ab150108): validated by immunostaining of HeLa cells (Abcam). Alexa 594 Donkey anti-rabbit IgG (Abcam, cat# ab150076): validated by immunostaining of HeLa cells (Abcam). For neutrophil depletion, rat GR1 antibody (Clone RB6-8C5, BioXCell, Cat#BE0075) was used: Validation by Bodogai et al, *Cancer Res* 75:3456-3465 (2015). For FACS analysis, we used: Rat anti-CD11b-Brilliant Violet 605 (clone M1/17, BioLegend), validated by staining myeloid immune cells in bone marrow (BioLegend). Rat anti-CD45-APC/Cy7 (clone, 30-F11, BioLegend), validated by staining mouse splenocytes (BioLegend). Rat anti-Ly6G-alexa Fluor 488 (clone 1A8, BioLegend), validated by staining mouse bone marrow cells (BioLegend). Rat anti-Ly6C-PerCP/Cy5.5 (clone HK1.4, BioLegend), validated by staining mouse bone marrow cells (BioLegend). Rat anti-Gr1-FITC (clone RB6-8C5, BioLegend), validated by staining mouse bone marrow cells (BioLegend). Rat anti-CD4 Pac Blue (clone GK1.5, BioLegend), validated by staining mouse splenocytes (BioLegend). Rat anti-CD8 α -PE/Cy7 (clone 53-6.7, BioLegend), validated by staining mouse splenocytes (BioLegend). Hamster anti-CD11c-APC (clone N418, BioLegend), validated by staining mouse splenocytes (BioLegend). Mouse anti-CD64-Brilliant Violet 421 (clone X54-5/7.1, BioLegend), validated by staining mouse bone marrow cells (BioLegend). Rat anti-SiglecF-Alexa Fluor 488 (clone E50-2440, BD Bioscience), validated by staining bone marrow cells (BD). Hamster anti-CD103 PE (clone 2E7, BioLegend), validated by staining mouse splenocytes (BioLegend). Hamster anti-TCR $\gamma\delta$ -PE (clone GL3, BioLegend), validated by staining mouse splenocytes (BioLegend). Rat anti-F4/80-FITC (clone BM8, BioLegend), validated by staining mouse peritoneal macrophages (BioLegend). Mouse anti-NK1.1-PerCP/Cy5.5 (clone PK136, BioLegend), validated by staining mouse splenocytes (BioLegend). Rat anti-B220-APC (clone RA3-6B2, BioLegend), validated by staining mouse splenocytes (BioLegend). Rat anti-CD3-PE/Cy7 (clone 17A2, BioLegend), validated by staining mouse splenocytes (BioLegend). Rat anti-CD24 Brilliant Violet 510 (clone M1/69, BioLegend), validated by staining mouse splenocytes (BioLegend). Hamster anti-TCR- β Brilliant Violet 421 (clone H57-597, BioLegend), validated by staining mouse splenocytes (BioLegend). Hamster anti-TCR V γ 1.1-APC (clone 2.11, BioLegend), validated by staining mouse lymph node cells (BioLegend). Hamster anti-TCR V γ 2-PE-Cy7 (clone UC3-10A6, eBioscience), validated by staining mouse lymph node cells (eBioscience). For FACS purification of lung cells: rat anti-CD3 ϵ -PE (clone 145-2C11, BioLegend), validated by mouse splenocyte staining (BioLegend). Rat anti-CD4-FITC (clone RM4-5, BioLegend), validated by mouse splenocyte staining (BioLegend). Rat anti-CD11b-Brilliant Violet 421 (clone M1/70, BioLegend), validated by mouse bone marrow staining (BioLegend). Hamster anti-CD11c-PE/Cy7 (clone N418, BioLegend), validated by staining mouse splenocytes (BioLegend). Rat anti-Ly6G-FITC (clone 1A8, BioLegend), validated by mouse bone marrow staining (BioLegend). Rat anti-CD19-PE (clone 6D5, BioLegend), validated by mouse splenocyte staining (BioLegend). Rat anti-CD45-APC/Cy7 (clone 30-F11, BioLegend), validated by mouse splenocyte staining (BioLegend). Hamster anti-TCR β -PE/Cy7 (clone H57-597, BioLegend), validated by mouse splenocyte staining (BioLegend). Hamster anti-TCR γ/δ -Brilliant Violet 421 (clone GL3, BioLegend), validated by mouse lymph node staining (BioLegend).

10. Eukaryotic cell lines

- State the source of each eukaryotic cell line used.
- Describe the method of cell line authentication used.
- Report whether the cell lines were tested for mycoplasma contamination.
- If any of the cell lines used are listed in the database of commonly misidentified cell lines maintained by [ICLAC](#), provide a scientific rationale for their use.

No eukaryotic cell lines were used in this study.

No eukaryotic cell lines were used in this study.

No eukaryotic cell lines were used in this study.

No commonly misidentified cell lines were used in this study.

► Animals and human research participants

Policy information about [studies involving animals](#); when reporting animal research, follow the [ARRIVE guidelines](#)

11. Description of research animals

Provide details on animals and/or animal-derived materials used in the study.

All animal experiments were approved and conducted according to Harvard Medical School institutional animal care and use committee (IACUC) guidelines or by the University of Calgary Animal Care Committee. Mice were bred and housed in a full barrier, specific pathogen free (SPF) animal facility at Harvard Medical School or an equivalent SPF facility at the University of Calgary. C57BL/6J, B6.Trpv1^{-/-}, B6.TCRd^{-/-}, B6.DTA^{+/+} and B6.129.Trpa1^{-/-} mice were purchased from Jackson Laboratories (Bar Harbor, ME, USA). Trpv1-Dtr mice on the C57BL/6 strain background were kindly provided by Dr. Mark Hoon (National Institutes of Health, MD, USA). Nav1.8-Cre mice on the C57BL/6 background were from Dr. John Wood (University College London, UK). Nav1.8-Cre^{+/-} mice were bred with B6.Dta^{+/+} mice to generate Nav1.8-Cre^{+/-}/Dta^{+/-} nociceptor ablated mice and control littermates (Nav1.8-Cre^{-/-}/Dta^{+/-}). For mouse experiments involving Trpv1 and Trpa1, heterozygous mice were bred to each other to produce WT (+/+), heterozygous (+/-), and knockout (-/-) littermate controls. Age-matched 8-14 week old male and female adult mice were used for experiments.

Policy information about [studies involving human research participants](#)

12. Description of human research participants

Describe the covariate-relevant population characteristics of the human research participants.

This study did not involve human research participants.

Flow Cytometry Reporting Summary

Form fields will expand as needed. Please do not leave fields blank.

▶ Data presentation

For all flow cytometry data, confirm that:

- 1. The axis labels state the marker and fluorochrome used (e.g. CD4-FITC).
- 2. The axis scales are clearly visible. Include numbers along axes only for bottom left plot of group (a 'group' is an analysis of identical markers).
- 3. All plots are contour plots with outliers or pseudocolor plots.
- 4. A numerical value for number of cells or percentage (with statistics) is provided.

▶ Methodological details

5. Describe the sample preparation.

For lung cellular FACS analysis, lungs from uninfected or infected animals were mechanically separated and minced into small pieces. The fine pieces of lung were digested in DMEM medium (Life Technologies) containing 2% FBS and 1.5 mg/ml collagenase D (Roche) at 37°C for 1 h with agitation (250 rpm). Following incubation, the cell mixture was passed through a 18 gauge needle 3 times, filtered through a 70 µm cell strainer (BD). Red blood cells were lysed for 20 minutes using a RBC lysis solution (eBioscience). Cells were blocked with Fc Block reagent, and incubated with a cocktail of staining antibodies for 30 minutes on ice in FACS buffer (PBS/2% FBS/1mM EDTA). For splenocyte FACS analysis, spleens were mashed, filtered through a 70 µm cell strainer (BD), lysed with RBC lysis buffer (eBioscience), treated with Fc Block reagent, resuspended in FACS buffer and stained for 30 minutes on ice. For broncho-alveolar lavage (BALF) cells, BALF was collected from euthanized animals by intratracheal instillation of 0.8 mL PBS twice, centrifuged at 4000 rpm for 7 min at 4°C, and cell pellet separated from supernatant, treated with RBC lysis solution (eBioscience), blocked with Fc block reagent, and resuspended in FACS buffer with a cocktail of antibodies for staining for 30 minutes on ice. All samples were washed twice and resuspended in PBS/2% PFA with 1 mM EDTA solution prior to flow cytometry. For FACS purification of lung-resident populations: antibodies against CD3ε (clone: 145-2C11), CD4 (clone: RM4-5), CD11b (clone: M1/70), Ly6G (clone: 1A8), CD19 (clone: 6D5), CD45 (clone: 30-F11), TCRβ (clone: H57-597) and TCRγ/δ (clone: GL3) from BioLegend. 7AAD from BD Pharmingen. Single cell suspensions were generated from lungs of 2-3 C57Bl/6J mice using lung dissociation kit (Miltenyi Biotec). Single-cell suspensions were incubated with CD90.2 MicroBeads (Miltenyi Biotec) and separated into CD90.2 positive and negative fractions. Both fractions were stained on ice with surface antibodies, live/dead marker 7AAD and sorted on a BD FACSAria (BD Biosciences). Different cell types were identified by the following gating strategies: B cells (7AAD-CD45+CD19+) and neutrophils (7AAD-CD45+CD11b+Ly6G+) were sorted from the pre-enriched CD90.2- cell fraction, while CD4+ T cells (7AAD-CD45+CD3+TCRβ+CD4+) and TCRγδ T cells (7AAD-CD45+CD3+TCRβ-TCRγδ+) were sorted from the pre-enriched CD90.2+ cell fraction.

6. Identify the instrument used for data collection.

Lung and spleen FACS analysis data was collected on BD LSR II analyzer

7. Describe the software used to collect and analyze the flow cytometry data.
8. Describe the abundance of the relevant cell populations within post-sort fractions.
9. Describe the gating strategy used.

(Bectin Dickinson). FACS purification of lung immune cells was accomplished in a BD FACSAria machine (Bectin Dickinson).

Data were collected with BD DIVA software, and files subsequently analyzed using FlowJo (Treestar, version 10.0.8r1)




We FACS purified several subsets of lung immune cells for quantitative realtime PCR, including neutrophils, TCRgd+ T cells, CD4+ T cells and B cells. The exact gating strategies used are given in Supplemental Figure 19.

For FACS analysis of lung cells and splenocytes: FSC vs. SSC gates were first used to exclude cell debris (bottom and far left) and to include most cells. The live cell stain (eFluor 450, ebioscience) was used to exclude dead cells for BALF and splenocyte analysis. Positive staining and gates for each fluorescent marker was defined by comparing full stainsets with a fluorescence minus one (FMO) control stainset that only lacked a particular marker antibody, but contained the rest of the antibodies in a mixed stain-set cocktail.

For FACS purification of lung cells: Single-cell suspensions were incubated with CD90.2 MicroBeads (Miltenyi Biotec) and separated into CD90.2 positive and negative fractions. Both fractions were stained on ice with surface antibodies, live/dead marker 7AAD and sorted on a BD FACSAria (BD Biosciences). Different cell types were identified by the following gating strategies: B cells (7AAD-CD45+CD19+) and neutrophils (7AAD-CD45+CD11b+Ly6G+) were sorted from the pre-enriched CD90.2- cell fraction, while CD4+ T cells (7AAD-CD45+CD3+TCRβ+CD4+) and TCRγδ T cells (7AAD-CD45+CD3+TCRβ-TCRγδ+) were sorted from the pre-enriched CD90.2+ cell fraction.

Tick this box to confirm that a figure exemplifying the gating strategy is provided in the Supplementary Information.

Author Correction: Nociceptor sensory neurons suppress neutrophil and $\gamma\delta$ T cell responses in bacterial lung infections and lethal pneumonia

Pankaj Baral, Benjamin D Umans , Lu Li, Antonia Wallrapp, Meghna Bist, Talia Kirschbaum, Yibing Wei, Yan Zhou, Vijay K Kuchroo, Patrick R Burkett, Bryan G Yipp , Stephen D Liberles and Isaac M Chiu 

Correction to: *Nature Medicine* <https://doi.org/10.1038/nm.4501>, published online 5 March 2018.

In the version of this article initially published, the line graph showing TNF- α levels in Fig. 2d was inadvertently duplicated. A graph of IL-6 levels should be shown in place of the duplication.

These results were also incorrectly described in the main text, which originally stated: “At an early time point of infection (6 h), RTX-treated mice showed higher induction of total inflammatory-protein levels in the bronchoalveolar lavage fluid (BALF) (Fig. 2c), as well as levels of the cytokines TNF- α and IL-6, and the chemokine CXCL-1 (Fig. 2d)”. This should instead read: “At an early time point of infection (6 h), RTX-treated mice showed higher induction of total inflammatory-protein levels in the bronchoalveolar lavage fluid (BALF) (Fig. 2c), as well as levels of the cytokine TNF- α and the chemokine CXCL-1 (Fig. 2d)”.

In the supplementary information initially posted online, incorrect bar graphs were presented in Supplementary Fig. 1b (VG, TRPV1+ data, top panel) and Supplementary Fig. 4b (DRG, CGRP+ data, middle panel).

The errors have been corrected in the HTML and PDF versions of this article.

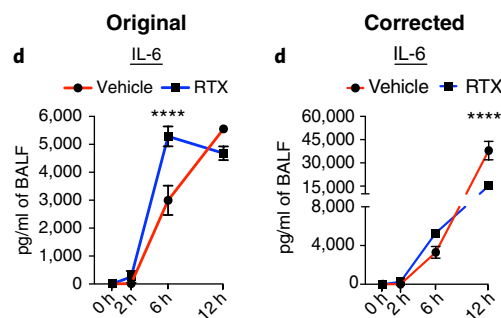
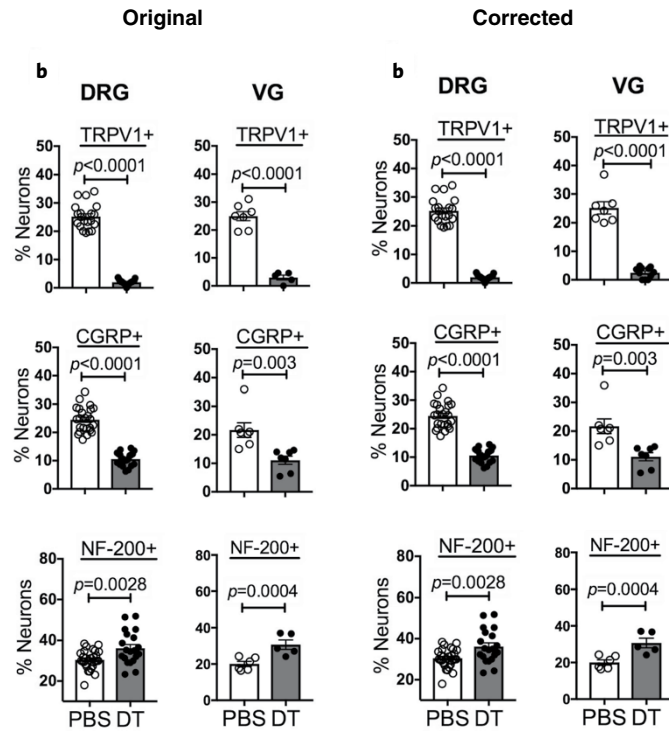


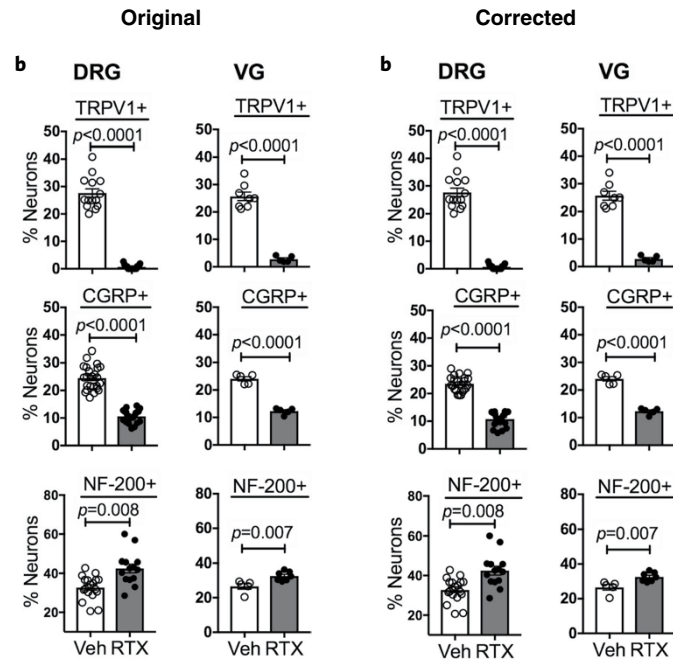
Fig. 2d | Original and corrected.

Published online: 16 July 2018

<https://doi.org/10.1038/s41591-018-0093-8>



Supplementary Fig. 1b | Original and corrected.



Supplementary Fig. 4b | Original and corrected.